Layered Control for Cooperative Locomotion of Two Quadrupedal Robots: Centralized and Distributed Approaches

Jeeseop Kim[1], Randall T. Fawcett[1], Vinay R. Kamidi[1], Aaron D. Ames[2], and Kaveh Akbari Hamed[1]

***Abstract*—This paper presents a layered control approach for real-time trajectory planning and control of robust cooperative locomotion by two holonomically constrained quadrupedal robots. A novel interconnected network of reduced-order models, based on the single rigid body (SRB) dynamics, is developed for trajectory planning purposes. At the higher level of the control architecture, two different model predictive control (MPC) algorithms are proposed to address the optimal control problem of the interconnected SRB dynamics: centralized and distributed MPCs. The distributed MPC assumes two local quadratic programs that share their optimal solutions according to a one-step communication delay and an agreement protocol. At the lower level of the control scheme, distributed nonlinear controllers are developed to impose the full-order dynamics to track the prescribed reduced-order trajectories generated by MPCs. The effectiveness of the control approach is verified with extensive numerical simulations and experiments for the robust and cooperative locomotion of two holonomically constrained A1 robots with different payloads on variable terrains and in the presence of disturbances. It is shown that the distributed MPC has a performance similar to that of the centralized MPC, while the computation time is reduced significantly.**

***Index Terms*—Legged Robots, Motion Control, Optimization and Optimal Control, Multi-Contact Whole-Body Motion Planning and Control**

I. Introduction

A. Motivation and Goal

HUMAN-centered communities, including factories, offices, and homes, are typically developed for humans who are bipedal walkers capable of stepping over gaps and walking up/down stairs. This motivates the development of collaborative legged robots that can cooperatively work with each other to assist humans in different aspects of their life, such as labor-intensive tasks, construction, manufacturing, and assembly. One of the most challenging and essential problems in deploying collaborative legged robots is *cooperative locomotion* in complex environments, wherein the collaboration between robots is described by holonomic constraints.

The work of J. Kim is supported by the National Science Foundation (NSF) under Grant 1924617. The work of K. Akbari Hamed is supported by the NSF under Grants 1924617 and 2024772. The work of R. T. Fawcett is supported by the NSF under Grant 2128948. The work of A. D. Ames is supported by the NSF under Grant 1924526.

[1]J. Kim, R. T. Fawcett, V. R. Kamidi, and K. Akbari Hamed (Corresponding Author) are with the Department of Mechanical Engineering, Virginia Tech, Blacksburg, VA 24061, USA, {jeeseop, randallf, vinay28, kavehakbarihamed}@vt.edu

[2]A. D. Ames is with the Department of Mechanical and Civil Engineering, California Institute of Technology, Pasadena, CA 91125, USA, ames@caltech.edu

Fig. 1. Snapshot illustrating holonomically constrained quadrupedal robots locomoting on gravel while carrying a payload of 4.53 (kg).

Cooperative locomotion with holonomic constraints arises in different applications of legged robots, such as cooperative transportation of payloads like social insects [1] (see Fig. 1), human-robot locomotion via prosthetic legs and exoskeletons [2]–[5], and human-robot locomotion via guide dog robots [6].

In recent years, important theoretical and technological advances have allowed for the successful control of multi-robot systems (MRSs) [7]–[9], including collaborative robotic arms with or without mobility [10]–[15], aerial vehicles [16]–[27], and ground vehicles [28]–[32]. In addition, distributed control algorithms, including distributed receding horizon control approaches, have been developed to address the motion planning of MRSs, see, e.g., [33]–[36]. Some recent works also address the control and planning of heterogeneous robot teams, including legged robots [37]–[39] but without holonomic constraints amongst the agents. However, the capabilities of cooperative legged locomotion have not been fully explored. In particular, collaborating legged robots can be described by high dimensional nonlinear dynamical systems with *hybrid* nature, and subject to underactuation and unilateral constraints, as opposed to most of the MRSs where the state-of-the-art algorithms have been deployed [40]. This complicates the design of trajectory planning and control approaches, both in centralized and distributed fashions, to guarantee each agent's robust stability while addressing the curse of dimensionality and respecting the holonomic and unilateral constraints.

Reduced-order (i.e., template) models provide low-dimensional realizations of full-order dynamical models of legged robots [41]. They can be integrated with convex optimization techniques and model predictive control (MPC)

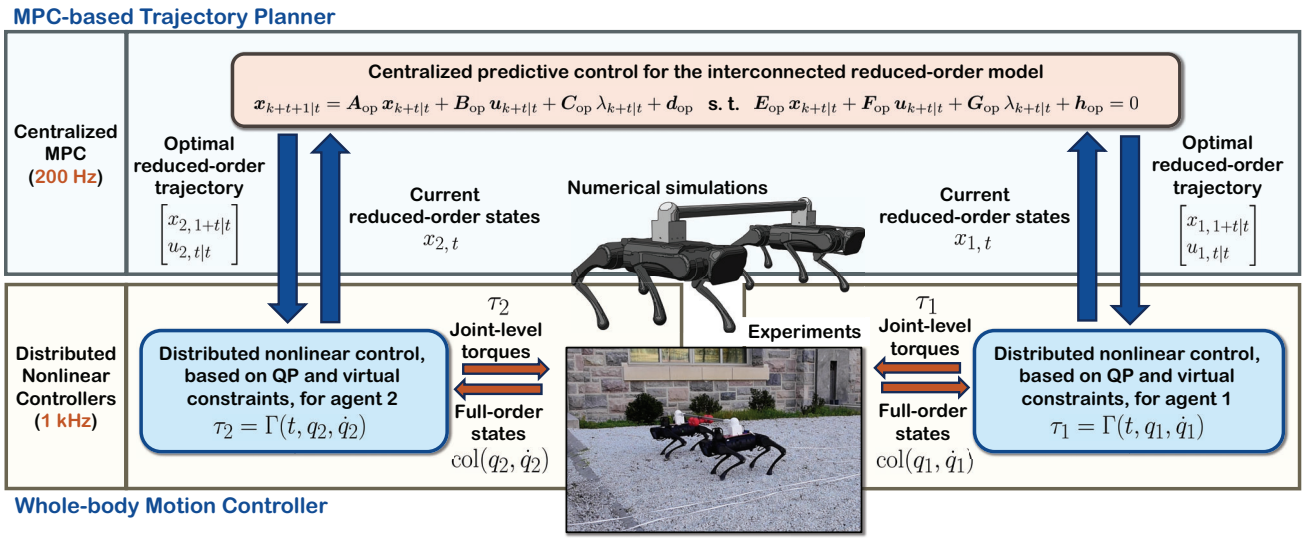

Fig. 2. Overview of the proposed layered control approach with the centralized MPC algorithm at the high level and distributed nonlinear controllers at the low level for cooperative locomotion.

approaches to enable gait planning for the existing legged robots. Some popular reduced-order models include the linear inverted pendulum (LIP) model [42], centroidal dynamics [43], and single rigid body (SRB) dynamics [44]–[46]. These template models have been used for real-time planning of different single-agent bipedal [47]–[50] and quadrupedal robots [44]–[46], [51]–[56]. In this paper, we aim to answer three *fundamental questions*. 1) How do we develop effective and interconnected reduced-order models that describe the cooperative locomotion of dynamic legged robots with holonomic constraints? 2) How do we develop computationally tractable predictive control algorithms in centralized and distributed manners for real-time planning of interconnected reduced-order models? And 3) How do we map optimal reduced-order trajectories to full-order and complex dynamical models of cooperative locomotion?

To address the above questions, this paper aims to develop mathematical foundations, experimentally implement, and comprehensively study the cooperative locomotion of two holonomically constrained dynamic legged robots. In particular, the *overarching goal* of this paper is to develop a layered control algorithm for the real-time trajectory planning and control of dynamic cooperative locomotion for two holonomically constrained legged-robotic systems. The higher layer of the proposed algorithm considers an innovative reduced-order model composed of two interconnected SRB dynamics subject to holonomic constraints for the planning problem. The paper develops novel centralized and distributed MPC algorithms for the planning purpose of interconnected SRB dynamics (see Figs. 2 and 3). These MPC algorithms address the real-time planning at the higher layer of the control hierarchy subject to the interaction terms and feasibility of the ground reaction forces (GRFs). The optimal reduced-order trajectories and GRFs, generated by the high-level MPCs, are then mapped to the full-order and complex dynamics via distributed nonlinear controllers at the low level for the whole-body motion control. The low-level nonlinear controllers are developed based on quadratic programming (QP) and input-output (I-O) linearization. The efficacy of the proposed layered control approach is validated via extensive experiments for robustly stable locomotion of two holonomically constrained A1 quadrupedal robots that cooperatively transport unknown payloads on different terrains and in the presence of disturbances (see Fig. 1). Here, we remark that the "robust stability" is defined in the context of maintaining balance during locomotion subject to various unknown disturbances and uneven terrains.

B. Related Work

In contrast to the existing collaborative MRSs introduced in Section I-A, collaborative legged robots are dynamical systems with high dimensionality, unilateral constraints, and hybrid nature that add further complexity to synthesizing planning and control algorithms. In addition, the interacting wrenches (forces/torques) between the agents, arising from holonomic constraints, must be carefully addressed to result in a robustly stable planner for cooperative legged locomotion. As a result, collaborative legged locomotion has not been studied to the same degree as other robotic systems. This paper marks the first experimental implementation in this context.

In the context of legged robots, the trajectory planning and control approaches can be sectioned into two categories: the ones using the full-order models and the others using the reduced-order models. Hybrid systems theory plays an important role in understanding and analyzing full-order dynamical models of legged locomotion [57]–[65]. Advanced nonlinear control algorithms such as hybrid reduction [66], controlled symmetries [67], transverse linearization [68], and hybrid zero dynamics (HZD) [69], [70] address the hybrid nature of full-order locomotion models. The HZD approach regulates some output functions, referred to as virtual constraints, with I-O linearization techniques [71] to coordinate the robot's links within a stride. This method can systematically address underactuation and its effectiveness has been validated for stable locomotion of different bipedal [72]–[76] and quadrupedal robots [77], [78] as well as powered prosthetic legs [4], [5].

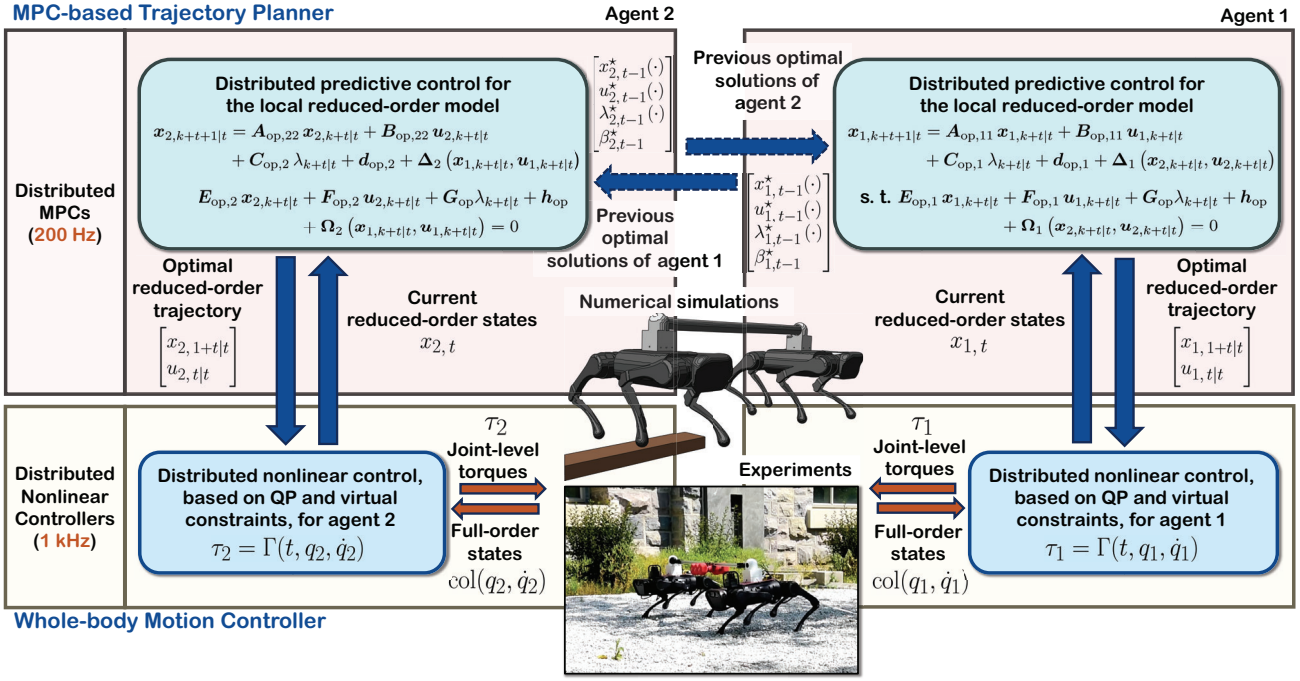

Fig. 3. Overview of the proposed layered control approach with the distributed MPC algorithms at the high level and distributed nonlinear controllers at the low level for cooperative locomotion.

The full-order gait planning is typically formulated as a nonlinear programming (NLP) problem that can be addressed with direct collocation techniques [75], [79]–[82]. Although the direct-collocation-based approaches generate optimal trajectories for full-order models of legged robots effectively, they *cannot* address real-time trajectory optimization of cooperative legged robots in complex environments.

In contrast to full-order models of legged locomotion, template models present simplified representations of legged robots with or without assumptions that significantly reduce the computational burden and complexity associated with trajectory optimization. Various template models, including LIP [42], SRB [44]–[46], and centroidal dynamics [43], have been successfully integrated with the MPC framework for the real-time planning of bipedal and quadrupedal robots [44]–[54], [56]. The main challenge with using template models is bridging the gap between reduced- and full-order models of locomotion arising from abstraction (e.g., ignoring the legs' dynamics in template models). In particular, one needs to translate the optimal reduced-order trajectories to the full-order joint positions and torques. Different hierarchical control algorithms have been proposed in the literature to close this gap, in which a whole-body motion controller is utilized at the low level to map the optimal trajectories, generated by the higher-level MPC, to the full-order dynamics. For instance, [45], [46] used a Jacobian mapping, [1], [53] used HZD-based controllers, [56] used robust MPC integrated with reinforcement learning, [83] used data-driven template models, and [55], [84] used joint space whole-body controllers.

Despite the success of the above methods on individual robots, it is unknown what reduced-order models can represent multi-agent-legged robots' dynamic and cooperative transportation effectively. In addition, it is unclear if the existing MPC techniques can address the real-time trajectory planning for the reduced-order models of cooperative locomotion with increased dimensionality. Moreover, it is unclear how the centralized MPC algorithms for such complex models can be decomposed into lower-dimensional distributed MPC algorithms considering the interaction terms.

C. Objectives and Contributions

The *objectives* and *key contributions* of this paper are as follows:

1) The paper presents an innovative network of two holonomically constrained SRB dynamics as an effective reduced-order model to capture the interaction wrenches between agents while dynamically stabilizing the motion during cooperative locomotion.
2) A layered control approach is proposed to robustly stabilize the cooperative locomotion of holonomically constrained quadrupedal robots. At the high level of the control hierarchy, two different MPC algorithms, based on QP, are proposed: centralized MPC and distributed MPC (see Figs. 2 and 3). The centralized MPC algorithm solves for the optimal state trajectory, GRFs, and interaction wrenches for the interconnected SRB dynamics. The distributed MPC algorithm assumes two local QPs that share their optimal solutions with a one-step communication delay. The distributed MPCs solve for the local states, local GRFs, and estimated local interaction wrenches according to an agreement protocol in the cost function. At the low level of the layered control architecture, distributed and nonlinear whole-body controllers, based on QP and virtual constraints, are utilized to impose the full-order dynamics to track the prescribed optimal reduced-order trajectories and GRFs, generated by the high-level MPCs.

3) Extensive numerical simulations are presented to evaluate the performance of the cooperative locomotion of two holonomically constrained A1 robots subject to various terrains and disturbances. A comparative analysis of the closed-loop systems with centralized and distributed MPC algorithms with more than 1000 randomly generated rough terrain profiles and external forces is presented. It is shown that the proposed distributed MPC algorithm has a performance similar to that of the centralized one, while the solve time is reduced by 70%.
4) The effectiveness of the proposed layered control algorithms (centralized and distributed) is verified with an extensive set of experiments for the blind and cooperative locomotion of two holonomically constrained A1 quadrupedal robots. The experiments include cooperative locomotion with different and unknown payloads on different terrains (covered with blocks, gravel, mulch, and slippery surfaces) and in the presence of external pushes and tethered pulling. Detailed robustness analysis is presented to experimentally evaluate the performance of the closed-loop system against the violations of assumptions made for the synthesis of the controller.

Our motivation for developing both the centralized and distributed MPCs is that the centralized MPC provides a substantial foundation to synthesize the distributed MPC. In particular, the distributed MPC is developed based on decomposing the centralized MPC subject to a one-step communication delay. Furthermore, the centralized MPC is used as a benchmark to comprehensively assess the performance of the distributed MPC, as the centralized MPC stabilizes cooperative locomotion through a relatively straightforward controller synthesis process. The distributed MPC presents an opportunity to significantly reduce the planner's computational burden arising from the interconnected model's complexity and hardware limitations. As a general guideline for selecting a controller, centralized MPC is often preferred due to its simplicity compared to its distributed counterpart. However, it is less scalable and supposes ideal (i.e., delay-free) communication between agents. In contrast, distributed MPC can overcome common communication and computational bottlenecks at the cost of increasing the complexity of the formulation.

The current work is different from our previous work [40] in that [40] did *not* consider real-time trajectory planning for the cooperative locomotion of two agents. It only addressed the stabilization of periodic trajectories generated *offline* for the hybrid model of cooperative locomotion and provided *no* experimental evaluation. The current work, however, develops centralized and distributed MPC algorithms for real-time trajectory planning while experimentally evaluating the results on hardware. The work also differs from [1] in that [1] formulated a centralized event-based MPC algorithm, similar to [53], for cooperative and *quasi-statistically* stable locomotion based on a network of interconnected LIP models while evaluating the results only in numerical simulations. The simple nature of the LIP model and event-based MPC reduced the computational burden by running the MPC only at the beginning of the continuous-time domains rather than every time sample. However, using the LIP model prohibits us from capturing the interaction torques due to the assumption of a concentrated point mass at the center of mass (COM), as we do not consider adding flywheels for simplicity. This model also restricts the generation of dynamic cooperative gaits because the center of pressure (COP) must always remain within the support polygon, limiting the system's full potential. The current work, however, presents faster centralized and distributed MPC algorithms for more complex networks of cooperative and *dynamically stable* locomotion based on SRB dynamics rather than LIP dynamics while numerically and experimentally evaluating the results. Moreover, the cooperative gaits of the current work are faster and more robust to uncertainties arising from external disturbances and unknown terrain profiles. Similarly, the present work is different from [85], [86] in that they employ centralized approaches based on the Zero Moment Point (ZMP) [87] criterion for generating quasi-statistically stable gaits for humanoid robots, whereas the current work develops both centralized and distributed planning and control approaches for dynamically stable cooperative gaits.

D. Organization

The paper is organized as follows. Section II develops interconnected SRB models as a reduced-order model of cooperative locomotion. Section III formulates centralized and distributed MPC-based trajectory planning algorithms. Section IV presents distributed nonlinear controllers for whole-body motion control. Section V provides a detailed and extensive set of numerical and experimental validations of the proposed layer control algorithm. In Section VI, we discuss the results and compare the performance of the centralized and distributed MPC algorithms. Section VII finally presents some concluding remarks and future research directions.

II. Reduced-Order Model of Cooperative Legged Locomotion

This section aims to address the reduced-order models that describe the cooperative locomotion of two holonomically constrained quadrupedal robots. The section assumes a rigid bar connected via ball joints to two points on the robots for carrying objects (see Fig. 1). These two points will be referred to as the *interaction points*. This assumption simplifies the analysis and results in a holonomic constraint, stating that the Euclidean distance between the interaction points is constant. However, the analysis of this section can be extended to more sophisticated connections, such as restricting the pitch or roll angles of the bar/load. In Section VI-D, we will experimentally show the robustness of the developed algorithms subject to these additional constraints.

In our notation, the subscript $i \in \mathcal{I} := \{1, 2\}$ represents the ith robot. We assume that $\{B_i\}$ is the local frame rigidly attached to the body of the agent i with its origin on the COM. The orientation of the frame $\{B_i\}$ with respect to the inertial world frame $\{O\}$ is denoted by $R_i \in \mathrm{SO}(3)$, where $\mathrm{SO}(3) := \{R \in \mathbb{R}^{3\times 3} \mid R^\top R = \mathbb{I}, \det(R) = 1\}$ is the special orthogonal group of order 3, and $\mathbb{I}$ represents the identity matrix. The Cartesian coordinates of the COM of agent i with respect to

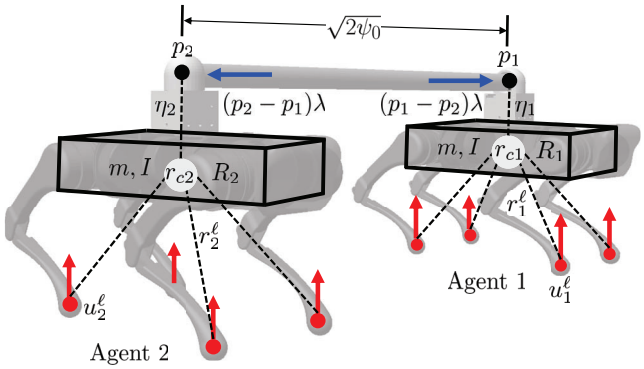

Fig. 4. Illustration of the interconnected SRB models for the cooperative locomotion of two quadrupedal robots.

$\{O\}$ are also represented by $r_{ci} := \text{col}(x_{ci}, y_{ci}, z_{ci}) \in \mathbb{R}^3$, where "col" denotes the column operator. Moreover, $\omega_i^{B_i} \in \mathbb{R}^3$ represents the angular velocity of agent i expressed in the body frame $\{B_i\}$. We assume that $p_i \in \mathbb{R}^3$ for $i \in \mathcal{I}$ represents Cartesian coordinates of the interaction points with respect to the inertial frame $\{O\}$, that is,

$$p_i = r_{ci} + R_i\, d_i^{B_i}, \tag{1}$$

where $d_i^{B_i} \in \mathbb{R}^3$ is a constant vector denoting the coordinates of the interaction points in the body frame $\{B_i\}$. For future purposes, we define $\eta_i := R_i\, d_i^{B_i}$ (see Fig. 4). We remark that the holonomic constraint between two agents can be described as a constraint on the Euclidean distance between the interaction points as follows:

$$\psi\left(r_{c1}, r_{c2}, R_1, R_2\right) := \frac{1}{2}\left\|p_1 - p_2\right\|^2 = \psi_0, \tag{2}$$

in which $\|\cdot\|$ denotes the 2-norm, and ψ_0 is a constant number, determined based on the length of the bar.

According to the principle of virtual work, one can consider $(p_1 - p_2)\,\lambda \in \mathbb{R}^3$ as the interaction force applied to agent 1 for some Lagrange multiplier $\lambda \in \mathbb{R}$ to be determined later (see again Fig. 4). Consequently, the net external wrench (f_i^{net} and τ_i^{net}) applied to agent $i \in \mathcal{I}$ can be expressed as follows:

$$\begin{bmatrix} f_i^{\text{net}} \\ \tau_i^{\text{net}} \end{bmatrix} = \sum_{\ell \in \mathcal{C}_i} \begin{bmatrix} \mathbb{I} \\ \widehat{r_i^\ell} \end{bmatrix} u_i^\ell + \begin{bmatrix} \mathbb{I} \\ \widehat{\eta_i} \end{bmatrix} (p_i - p_j)\,\lambda, \tag{3}$$

where $j \neq i \in \mathcal{I}$ denotes the index of the other agent and the hat map $\widehat{(\cdot)} : \mathbb{R}^3 \to \mathfrak{so}(3)$ represents the skew-symmetric operator with the property $\widehat{x}\, y = x \times y$ for all $x, y \in \mathbb{R}^3$. In (3), the superscript $\ell \in \mathcal{C}_i$ denotes the index of the contacting legs with the ground, $\mathcal{C}_i$ represents the set of contacting legs for the agent i, and $u_i^\ell \in \mathbb{R}^3$ denotes the GRF at the contacting leg ℓ for the agent i. In addition, $r_i^\ell \in \mathbb{R}^3$ represents the position of each contacting leg with respect to the COM of agent i, that is, $r_i^\ell = r_{\text{foot},i}^\ell - r_{ci}$, where $r_{\text{foot},i}^\ell$ is the position of the contacting foot ℓ of the agent i with respect to $\{O\}$.

By taking the *local state variables* for the agent $i \in \mathcal{I}$ as

$$\boldsymbol{x}_i := \text{col}\left(r_{ci}, \dot{r}_{ci}, \text{vec}(R_i), \omega_i^{B_i}\right) \in \mathbb{R}^{18}, \tag{4}$$

the *global state variables* can be defined as

$$\boldsymbol{x} := \text{col}\left(\boldsymbol{x}_1, \boldsymbol{x}_2\right), \tag{5}$$

where "vec" represents the vectorization operator. The *global control inputs* can be defined as $\boldsymbol{u} := \text{col}(\boldsymbol{u}_1, \boldsymbol{u}_2)$, where $\boldsymbol{u}_i$ denotes the *local control inputs* (i.e., GRFs) for agent i, i.e.,

$$\boldsymbol{u}_i := \text{col}\left\{u_i^\ell \,|\, \ell \in \mathcal{C}_i\right\}. \tag{6}$$

By differentiating the holonomic constraint (2), one can get

$$\dot{\psi}(\boldsymbol{x}) = (p_1 - p_2)^\top (\dot{p}_1 - \dot{p}_2) = 0, \tag{7}$$

and hence, the *state manifold* can be expressed as $\boldsymbol{\mathcal{X}} := \{\boldsymbol{x} \in \mathbb{R}^{36} |\, R_i \in \text{SO(3)},\, i \in \mathcal{I},\, \psi(\boldsymbol{x}) = \psi_0, \dot{\psi}(\boldsymbol{x}) = 0\}$. Finally, the interconnected SRB dynamics can be expressed as

$$\dot{\boldsymbol{x}} = \boldsymbol{f}(\boldsymbol{x}, \boldsymbol{u}, \lambda) := \begin{bmatrix} \dot{r}_{c1} \\ \frac{f_1^{\text{net}}}{m} - g \\ \text{vec}(R_1\, \widehat{\omega_1^{B_1}}) \\ I^{-1}\left(R_1^\top \tau_1^{\text{net}} - \widehat{\omega_1^{B_1}}\, I\, \omega_1^{B_1}\right) \\ \dot{r}_{c2} \\ \frac{f_2^{\text{net}}}{m} - g \\ \text{vec}(R_2\, \widehat{\omega_2^{B_2}}) \\ I^{-1}\left(R_2^\top \tau_2^{\text{net}} - \widehat{\omega_2^{B_2}}\, I\, \omega_2^{B_2}\right) \end{bmatrix}, \tag{8}$$

where m and $I \in \mathbb{R}^{3\times3}$ denote the total mass and the fixed moment of inertia in the body frame for each agent, respectively, and g represents the constant gravitational vector. We remark that the kinematics relations in (8) are expressed as $\dot{R}_i = R_i\, \widehat{\omega_i^{B_i}}$ for $i \in \mathcal{I}$. The rotational dynamics can be further expressed as Euler's equation $I\, \dot{\omega}_i^{B_i} + \widehat{\omega_i^{B_i}}\, I\, \omega_i^{B_i} = R_i^\top \tau_i^{\text{net}}$. The net external wrench (f_i^{net} and τ_i^{net}) in (3) can be plugged in (8) to reveal the Lagrange multiplier, λ, and local control inputs, $\boldsymbol{u}_i$, in the interconnected SRB dynamics. We note that in (8), $\boldsymbol{f} : \boldsymbol{\mathcal{X}} \times \boldsymbol{\mathcal{U}} \times \mathbb{R} \to \text{T}\boldsymbol{\mathcal{X}}$ is smooth with

$$\boldsymbol{\mathcal{U}} := \underbrace{\mathcal{FC} \times \cdots \times \mathcal{FC}}_{m_u - \text{times}} \subset \mathbb{R}^{3m_u} \tag{9}$$

being the *admissible set of control inputs*, where m_u denotes the total number of contacting legs with the ground (e.g., $m_u = 4$ for cooperative trot), $\mathcal{FC} := \{\text{col}(f_x, f_y, f_z) \,|\, f_z > 0,\, |f_x| \leq \frac{\mu}{\sqrt{2}} f_z,\, |f_y| \leq \frac{\mu}{\sqrt{2}} f_z\}$ represents the linearized friction cone for some friction coefficient μ, and $\text{T}\boldsymbol{\mathcal{X}}$ is the tangent bundle of the state manifold $\boldsymbol{\mathcal{X}}$. We remark that the admissible set of control inputs, $\boldsymbol{\mathcal{U}}$, is a condition to guarantee the non-slippage at the ground contact point of each leg.

In order to make the manifold $\boldsymbol{\mathcal{X}}$ invariant under the flow of (8), one would need to choose the Lagrange multiplier λ to satisfy the holonomic constraint. In particular, differentiating (7) according to (1) and $\dot{R}_i = R_i\, \widehat{\omega_i^{B_i}}$ results in

$$\begin{aligned} \ddot{\psi}(\boldsymbol{x}, \boldsymbol{u}, \lambda) &= (p_1 - p_2)^\top (\ddot{p}_1 - \ddot{p}_2) + \|\dot{p}_1 - \dot{p}_2\|^2 \\ &= (p_1 - p_2)^\top \Big\{ \ddot{r}_{c1} - \ddot{r}_{c2} \\ &+ R_1 \left(\widehat{\omega_1^{B_1}}\right)^2 d_1^{B_1} - R_2 \left(\widehat{\omega_2^{B_2}}\right)^2 d_2^{B_2} \\ &+ R_1\, \widehat{\dot{\omega}_1^{B_1}} d_1^{B_1} - R_2\, \widehat{\dot{\omega}_2^{B_2}} d_2^{B_2} \Big\} \\ &+ \|\dot{p}_1 - \dot{p}_2\|^2 = 0. \end{aligned} \tag{10}$$

This latter equation, together with the equations of motion (8) and (3), results in λ being a function of $(\boldsymbol{x}, \boldsymbol{u})$. However, replacing this nonlinear expression for λ in (8) can make the original dynamics (8) more nonlinear and complex. Furthermore, this can numerically complicate the Jacobian linearization of $\dot{\boldsymbol{x}} = \boldsymbol{f}(\boldsymbol{x}, \boldsymbol{u}, \lambda(\boldsymbol{x}, \boldsymbol{u}))$ when formulating the trajectory planning problem as a convex MPC in Section III. Alternatively, we pursue a computationally effective approach by considering $\dot{\boldsymbol{x}} = \boldsymbol{f}(\boldsymbol{x}, \boldsymbol{u}, \lambda)$ subject to the equality constraint $\ddot{\psi}(\boldsymbol{x}, \boldsymbol{u}, \lambda) = 0$ within the optimal control problem formulation. More specifically, the decision variables for the MPC include the trajectories of $(\boldsymbol{x}, \boldsymbol{u}, \lambda)$ over the control horizon, and the MPC will satisfy the equality constraint. The other advantage of this technique is that the interconnected SRB dynamics can be integrated with the variational-based approach of [45], [46] to linearize and then discretize the dynamics such that the rotation matrices $R_i, i \in \mathcal{I}$ approximately evolve on SO(3).

To clarify this latter point, following [46], we introduce a new set of local state variables for the agent $i \in \mathcal{I}$ with the abuse of notation as

$$\boldsymbol{x}_i := \text{col}\left(r_{ci}, \dot{r}_{ci}, \xi_i, \omega_i^{B_i}\right) \in \mathbb{R}^{12}. \tag{11}$$

Here, $\xi_i \in \mathbb{R}^3$ is a vector used to approximate the rotation matrix R_i around an operating point $R_{i,\text{op}}$ using the Taylor series expansion as follows:

$$R_i = R_{i,\text{op}} \exp(\widehat{\xi_i}) \approx R_{i,\text{op}} \left(\mathbb{I} + \widehat{\xi_i}\right). \tag{12}$$

For small changes in the rotation matrix at each time sample, ξ_i remains small. Hence, (12) is a reasonable approximation. The approach of [46] has linearized the SRB dynamics subject to GRFs without interaction forces. Hence, one must extend the technique by obtaining the Taylor series expansion for the additional wrench terms in (3) arising from the interaction. For this purpose, (12) can be applied to (8) to represent the nonlinear and interconnected SRB dynamics utilizing the new state variables found in (11). Then, we can derive the Jacobian linearization of the smooth nonlinear dynamics (8) subject to the new state variables in (11). These dynamics can then be discretized using the forward Euler method, which results in a discrete and linear system to predict the future states as follows:

$$\boldsymbol{x}_{k+t+1|t} = \boldsymbol{A}_{\text{op}}\, \boldsymbol{x}_{k+t|t} + \boldsymbol{B}_{\text{op}}\, \boldsymbol{u}_{k+t|t} + \boldsymbol{C}_{\text{op}}\, \lambda_{k+t|t} + \boldsymbol{d}_{\text{op}}, \tag{13}$$

for all $k = 0, 1, \cdots, N-1$ and with the initial condition $\boldsymbol{x}_{t|t} = \boldsymbol{x}_t$. Here, $\boldsymbol{x} \in \mathbb{R}^{24}$ denotes the global state variables, N represents the control horizon, and $(\boldsymbol{x}_{k+t|t}, \boldsymbol{u}_{k+t|t}, \lambda_{k+t|t})$ denotes the tuple of the predicted global states, global inputs (i.e., GRFs), and Lagrange multiplier at time $k+t$ computed at time t. Furthermore, $\boldsymbol{A}_{\text{op}} := \partial \boldsymbol{f}/\partial \boldsymbol{x}(\boldsymbol{x}_t, \boldsymbol{u}_{t-1}, \lambda_{t-1}) \in \mathbb{R}^{24\times 24}$, $\boldsymbol{B}_{\text{op}} := \partial \boldsymbol{f}/\partial \boldsymbol{u}(\boldsymbol{x}_t, \boldsymbol{u}_{t-1}, \lambda_{t-1}) \in \mathbb{R}^{24\times 3m_u}$, $\boldsymbol{C}_{\text{op}} := \partial \boldsymbol{f}/\partial \lambda(\boldsymbol{x}_t, \boldsymbol{u}_{t-1}, \lambda_{t-1}) \in \mathbb{R}^{24}$, and $\boldsymbol{d}_{\text{op}} := \boldsymbol{f}(\boldsymbol{x}_t, \boldsymbol{u}_{t-1}, \lambda_{t-1}) - \boldsymbol{A}_{\text{op}}\, \boldsymbol{x}_t - \boldsymbol{B}_{\text{op}}\, \boldsymbol{u}_{t-1} - \boldsymbol{C}_{\text{op}}\, \lambda_{t-1} \in \mathbb{R}^{24}$ are the Jacobian matrices and offset term evaluated around the current operating point $(\boldsymbol{x}_t, \boldsymbol{u}_{t-1}, \lambda_{t-1})$ that can be either computed via symbolic calculus or the approach of [46].

The approximation in (12) only ensures that the rotation matrices approximately evolve on SO(3). To guarantee that the state predictions in (13) belong to the tangent space of the state manifold at the operating point (i.e., $\text{T}_{\text{op}}\boldsymbol{\mathcal{X}}$), we first define the following equality constraint

$$\boldsymbol{\Psi}(\boldsymbol{x}, \boldsymbol{u}, \lambda) := \begin{bmatrix} \psi(\boldsymbol{x}) - \psi_0 \\ \dot{\psi}(\boldsymbol{x}) \\ \ddot{\psi}(\boldsymbol{x}, \boldsymbol{u}, \lambda) \end{bmatrix} = 0. \tag{14}$$

Then, analogous to the technique used for the linearization of the interconnected dynamics, the equality constraint (14) can be approximated around the operating point as follows:

$$\boldsymbol{E}_{\text{op}}\, \boldsymbol{x}_{k+t|t} + \boldsymbol{F}_{\text{op}}\, \boldsymbol{u}_{k+t|t} + \boldsymbol{G}_{\text{op}}\, \lambda_{k+t|t} + \boldsymbol{h}_{\text{op}} = 0 \tag{15}$$

to ensure that $\boldsymbol{\Psi}(\boldsymbol{x}_{k+t|t}, \boldsymbol{u}_{k+t|t}, \lambda_{k+t|t}) \equiv 0$. Here, $\boldsymbol{E}_{\text{op}} := \partial \boldsymbol{\Psi}/\partial \boldsymbol{x}(\boldsymbol{x}_t, \boldsymbol{u}_{t-1}, \lambda_{t-1}) \in \mathbb{R}^{3\times 24}$, $\boldsymbol{F}_{\text{op}} := \partial \boldsymbol{\Psi}/\partial \boldsymbol{u}(\boldsymbol{x}_t, \boldsymbol{u}_{t-1}, \lambda_{t-1}) \in \mathbb{R}^{3\times 3m_u}$, $\boldsymbol{G}_{\text{op}} := \partial \boldsymbol{\Psi}/\partial \lambda(\boldsymbol{x}_t, \boldsymbol{u}_{t-1}, \lambda_{t-1}) \in \mathbb{R}^3$, and $\boldsymbol{h}_{\text{op}} := \boldsymbol{\Psi}(\boldsymbol{x}_t, \boldsymbol{u}_{t-1}, \lambda_{t-1}) - \boldsymbol{E}_{\text{op}}\, \boldsymbol{x}_t - \boldsymbol{F}_{\text{op}}\, \boldsymbol{u}_{t-1} - \boldsymbol{G}_{\text{op}}\, \lambda_{t-1} \in \mathbb{R}^3$ are proper matrices and vectors.

***Remark** 1:* As the nature of the holonomic constraints between the agents becomes more complex, the procedure for obtaining the corresponding prediction model and equality constraints becomes computationally expensive. However, our experimental results in Section VI-D will indicate that the proposed layered control approach, developed based on the assumption of holonomic constraints in (2), can robustly stabilize cooperative locomotion subject to uncertainties in the constraints (e.g., limiting the pitch angles of the ball joints).

III. MPC-Based Trajectory Planning

This section aims to formulate the trajectory planning problem for cooperative locomotion as centralized and distributed MPC algorithms.

A. Centralized MPC

We will consider a locomotion pattern for the agents, described by the directed cycle $\mathcal{G}(\mathcal{V}, \mathcal{E})$, where $\mathcal{V}$ and $\mathcal{E} \subset \mathcal{V} \times \mathcal{V}$ represent the sets of vertices and edges, respectively. The vertices denote the continuous-time domains of locomotion, and the edges represent the discrete-time transitions between the continuous-time domains.

***Assumption** 1:* The higher-level MPC is aware of the current stance legs at every time sample t, assuming that the stance leg configuration does not change throughout the control horizon.

***Remark** 2:* Assumption 1 is *not* restrictive and simplifies the optimal control problem of (13) subject to (15) over the control horizon. Otherwise, one would need to consider the optimal control problem for a piecewise affine (PWA) system [88, Chap. 16] subject to different switching times. In particular, if the stance leg configuration changes within the control horizon, the existing control inputs (i.e., GRFs) for the prediction model (13) are no longer available, and new control inputs need to be considered for the following continuous-time domain. This makes the dynamics of the system switching (PWA), and the optimal control problem becomes complex.

We are now in a position to present the following centralized MPC algorithm for the cooperative locomotion

$$\begin{aligned}\min_{(\boldsymbol{x}(\cdot),\boldsymbol{u}(\cdot),\lambda(\cdot))} \; & p\left(\boldsymbol{x}_{t+N|t}\right)+\sum_{k=0}^{N-1}\mathcal{L}\left(\boldsymbol{x}_{k+t|t},\boldsymbol{u}_{k+t|t},\lambda_{k+t|t}\right)\\ \text{s.t.} \quad & \text{Prediction model (13)}\\ & \text{Equality constraints (15)}\\ & \boldsymbol{u}_{k+t|t}\in\boldsymbol{\mathcal{U}},\quad k=0,1,\cdots,N-1,\end{aligned}\tag{16}$$

where the equality constraints for the MPC arise from a) the prediction model (13) to address the interconnected SRB dynamics with the initial condition of $\boldsymbol{x}_{t|t}=\boldsymbol{x}_t$, and b) the holonomic constraints (15) (see Fig. 2). Here, the centralized MPC solves for the optimal trajectories of the global states, global inputs, and the Lagrange multiplier encoded in $(\boldsymbol{x}(\cdot),\boldsymbol{u}(\cdot),\lambda(\cdot))$ to retain the sparsity structure of [89], where $\boldsymbol{x}(\cdot):=\text{col}\{\boldsymbol{x}_{k+t|t}\,|\,k=1,\cdots,N\}$, $\boldsymbol{u}(\cdot):=\text{col}\{\boldsymbol{u}_{k+t|t}\,|\,k=0,1,\cdots,N-1\}$, and $\lambda(\cdot):=\text{col}\{\lambda_{k+t|t}\,|\,k=0,1,\cdots,N-1\}$. The terminal and stage cost functions in (16) are then taken as $p(\boldsymbol{x}_{t+N|t}):=\|\boldsymbol{x}_{t+N|t}-\boldsymbol{x}^{\text{des}}_{t+N|t}\|^2_{\boldsymbol{P}}$ for a positive definite matrix $\boldsymbol{P}$ and $\mathcal{L}(\boldsymbol{x}_{k+t|t},\boldsymbol{u}_{k+t|t},\lambda_{k+t|t}):=\|\boldsymbol{x}_{k+t|t}-\boldsymbol{x}^{\text{des}}_{k+t|t}\|^2_{\boldsymbol{Q}}+\|\boldsymbol{u}_{k+t|t}\|^2_{\boldsymbol{R}_u}+\|\lambda_{k+t|t}\|^2_{\boldsymbol{R}_\lambda}$ for some desired trajectory $\boldsymbol{x}^{\text{des}}(\cdot)$ and some positive definite matrices $\boldsymbol{Q}$ and $\boldsymbol{R}_u$, and a positive scalar $\boldsymbol{R}_\lambda$. Finally, the inequality constraints of (16) represent the feasibility of the GRFs for two agents.

***Remark** 3:* The MPC in (16) addresses the trajectory planning problem over the current continuous-time domain. In particular, we do not include the following domain (i.e. next continuous-time domain) for prediction purposes in light of Assumption 1. We employ Raibert's heuristic [90, Eq. (2.4), pp. 46] to plan for the upcoming footholds of each agent. The centralized MPC has $(25{+}3\,m_u)\,N$ decision variables. Finally, the MPC problem (16) solves for the optimal trajectories of the state variables $\boldsymbol{x}^\star(\cdot)$, control inputs $\boldsymbol{u}^\star(\cdot)$, and Lagrange multiplier $\lambda^\star(\cdot)$. However, the high-level MPC only applies the first element of the optimal state and control sequence, i.e., $(\boldsymbol{x}^\star_{t+1|t},\boldsymbol{u}^\star_{t|t})$, to the low-level controller for tracking while discarding $\lambda^\star_{t|t}$ (see Fig. 2).

***Remark** 4:* The centralized MPC algorithm of this paper is different from [1]. In particular, according to the simple nature of the LIP dynamics, [1] eliminates the Lagrange multipliers and presents a simple interconnected network of LIP dynamics. Furthermore, the centralized MPC algorithm of [1] is solved in an event-based manner (i.e., at the beginning of each gait). The Lagrange multipliers cannot be eliminated from the interconnected SRB dynamics in the current work due to the complexity of the reduced-order model. Hence, the centralized MPC algorithm in (16) solves for the optimal trajectory as well as the optimal Lagrange multipliers subject to the holonomic constraints (15). In addition, the MPC algorithm in (16) is solved at every time sample rather than the event-based manner of [1] to address more dynamic motions.

B. Distributed MPC

This section aims to develop a network of distributed MPCs with a smaller number of decision variables that plan for the cooperative locomotion of two holonomically constrained quadrupedal robots. For this purpose, the state matrices and vectors in (13) can be partitioned as follows:

$$\begin{aligned}&\boldsymbol{A}_{\text{op}}=\begin{bmatrix}\boldsymbol{A}_{\text{op},11}\,\boldsymbol{A}_{\text{op},12}\\ \boldsymbol{A}_{\text{op},21}\,\boldsymbol{A}_{\text{op},22}\end{bmatrix},\ \boldsymbol{B}_{\text{op}}=\begin{bmatrix}\boldsymbol{B}_{\text{op},11}\,\boldsymbol{B}_{\text{op},12}\\ \boldsymbol{B}_{\text{op},21}\,\boldsymbol{B}_{\text{op},22}\end{bmatrix},\\ &\boldsymbol{C}_{\text{op}}=\begin{bmatrix}\boldsymbol{C}_{\text{op},1}\\ \boldsymbol{C}_{\text{op},2}\end{bmatrix},\qquad \boldsymbol{d}_{\text{op}}=\begin{bmatrix}\boldsymbol{d}_{\text{op},1}\\ \boldsymbol{d}_{\text{op},2}\end{bmatrix},\end{aligned}\tag{17}$$

with $\boldsymbol{A}_{\text{op},ii},\boldsymbol{A}_{\text{op},ij}\in\mathbb{R}^{12\times 12}$, $\boldsymbol{B}_{\text{op},ii},\boldsymbol{B}_{\text{op},ij}\in\mathbb{R}^{12\times\frac{3}{2}m_u}$, $\boldsymbol{C}_{\text{op},i}\in\mathbb{R}^{12}$, and $\boldsymbol{d}_{\text{op},i}\in\mathbb{R}^{12}$ for all $i\neq j\in\mathcal{I}$, where the off-diagonal portions of the matrices represent the interaction terms between agents, and the rest are assigned to the local dynamics. More specifically, from (13) and (17), the local predictions of the agent $i\in\mathcal{I}$ can be expressed as:

$$\begin{aligned}\boldsymbol{x}_{i,k+t+1|t}=&\,\boldsymbol{A}_{\text{op},ii}\,\boldsymbol{x}_{i,k+t|t}+\boldsymbol{B}_{\text{op},ii}\,\boldsymbol{u}_{i,k+t|t}\\ &+\boldsymbol{C}_{\text{op},i}\,\lambda_{k+t|t}+\boldsymbol{d}_{\text{op},i}+\boldsymbol{\Delta}_i\left(\boldsymbol{x}_{j,k+t|t},\boldsymbol{u}_{j,k+t|t}\right),\end{aligned}\tag{18}$$

where $j\neq i\in\mathcal{I}$, and $(\boldsymbol{x}_{i,k+t|t},\boldsymbol{u}_{i,k+t|t})$ denotes the tuple of local states and inputs for agent i at time $k+t$ computed at time t. In addition,

$$\boldsymbol{\Delta}_i\left(\boldsymbol{x}_{j,k+t|t},\boldsymbol{u}_{j,k+t|t}\right):=\boldsymbol{A}_{\text{op},ij}\,\boldsymbol{x}_{j,k+t|t}+\boldsymbol{B}_{\text{op},ij}\,\boldsymbol{u}_{j,k+t|t},\tag{19}$$

represents the interaction term on agent i influenced by agent j. Similarly, the equality constraints (15) can be partitioned as follows:

$$\begin{aligned}&\boldsymbol{E}_{\text{op},i}\,\boldsymbol{x}_{i,k+t|t}+\boldsymbol{F}_{\text{op},i}\,\boldsymbol{u}_{i,k+t|t}+\boldsymbol{G}_{\text{op}}\lambda_{k+t|t}+\boldsymbol{h}_{\text{op}}\\ &\qquad+\boldsymbol{\Omega}_i\left(\boldsymbol{x}_{j,k+t|t},\boldsymbol{u}_{j,k+t|t}\right)=0,\end{aligned}\tag{20}$$

in which $\boldsymbol{E}_{\text{op},i}\in\mathbb{R}^{3\times 12}$ and $\boldsymbol{F}_{\text{op},i}\in\mathbb{R}^{3\times\frac{m_u}{2}}$ are the corresponding columns of $(\boldsymbol{E}_{\text{op}},\boldsymbol{F}_{\text{op}})$, and

$$\boldsymbol{\Omega}_i\left(\boldsymbol{x}_{j,k+t|t},\boldsymbol{u}_{j,k+t|t}\right):=\boldsymbol{E}_{\text{op},j}\,\boldsymbol{x}_{j,k+t|t}+\boldsymbol{G}_{\text{op},j}\,\boldsymbol{u}_{j,k+t|t}$$

for $j\neq i$. Motivated by the inherent limitation of the distributed QP problems, one would need to estimate the interaction terms $\boldsymbol{\Delta}_i$ and $\boldsymbol{\Omega}_i$, $i\in\mathcal{I}$ to solve for local QPs. For this purpose, we make the following assumption.

***Assumption** 2 (One-Step Communication Protocol):* At every time sample t, each local MPC has access to the optimal solution of the other local MPC at time $t-1$. More specifically, the local MPCs share their previous optimal solutions over the network.

We remark that Assumption 2 is not restrictive. Numerical simulations and experimental validations in Section V with various unknown disturbances and multiple uneven terrains show that the proposed trajectory planners can address robust cooperative locomotion with this assumption while solving the MPC every 5 (ms). From Assumption 2, we can estimate the interaction terms $\boldsymbol{\Delta}_i$ and $\boldsymbol{\Omega}_i$ in (18) and (20) using the previous optimal solutions, that is,

$$\begin{aligned}\boldsymbol{\Delta}_i\left(\boldsymbol{x}_{j,k+t|t},\boldsymbol{u}_{j,k+t|t}\right)&\approx\boldsymbol{\Delta}_i\left(\boldsymbol{x}^\star_{j,k+t|t-1},\boldsymbol{u}^\star_{j,k+t|t-1}\right)\\ \boldsymbol{\Omega}_i\left(\boldsymbol{x}_{j,k+t|t},\boldsymbol{u}_{j,k+t|t}\right)&\approx\boldsymbol{\Omega}_i\left(\boldsymbol{x}^\star_{j,k+t|t-1},\boldsymbol{u}^\star_{j,k+t|t-1}\right),\end{aligned}\tag{21}$$

in which $\boldsymbol{x}^\star_{j,k+t|t-1}$ and $\boldsymbol{u}^\star_{j,k+t|t-1}$ denote the optimal solution from the local QP j for time $k+t$ computed at time $t-1$ for $k=0,1,\cdots,N-1$. We remark that as the QP j does not

plan for $\boldsymbol{u}_{N-1+t|t-1}$, we let $\boldsymbol{u}^{\star}_{N-1+t|t-1} = 0$. The assumption in (21) estimates the interaction terms in the local dynamics and equality constraints based on the optimal values from the local QP j at the previous time sample. With this assumption, the local MPC i needs to optimally solve for its own local state trajectory $\boldsymbol{x}_i(\cdot)$, local control trajectory $\boldsymbol{u}_i(\cdot)$, and the Lagrange multiplier trajectory $\lambda(\cdot)$. However, as the Lagrange multiplier λ is common between the decision variables of two local MPCs, they need to reach a consensus over time for the optimal λ value.

To address the consensus problem, we develop an agreement protocol as follows. The cost function of the centralized MPC (16) can be written as the sum of individual terms, i.e.,

$$\mathcal{J}_1\left(\boldsymbol{x}_1(\cdot), \boldsymbol{u}_1(\cdot)\right) + \mathcal{J}_2\left(\boldsymbol{x}_2(\cdot), \boldsymbol{u}_2(\cdot)\right) + \mathcal{J}_\lambda\left(\lambda(\cdot)\right). \tag{22}$$

We assume that each local QP estimates its own trajectory of the Lagrange multiplier, denoted by $\lambda_i(\cdot)$. We then propose the following distributed MPC for agent $i \in \mathcal{I}$

$$\begin{aligned}
\min_{(\boldsymbol{x}_i(\cdot), \boldsymbol{u}_i(\cdot), \lambda_i(\cdot))} \; & \mathcal{J}_i\left(\boldsymbol{x}_i(\cdot), \boldsymbol{u}_i(\cdot)\right) + \mathcal{J}_\lambda\left(\lambda_i(\cdot)\right) \\
& + w \sum_{k=0}^{N-1} \left\| \lambda_{i,k+t|t} - a_{ii}\, \lambda^{\star}_{i,k+t|t-1} - a_{ij}\, \lambda^{\star}_{j,k+t|t-1} \right\|^2 \\
& + \beta^{\star\top}_{j,t-1}\, \mathcal{K}_{j,i} \begin{bmatrix} \boldsymbol{x}_i(\cdot) \\ \boldsymbol{u}_i(\cdot) \end{bmatrix} + \beta^{\star\top}_{j,t-1}\, \mathcal{K}_{j,\lambda}\, \lambda_i(\cdot) \\
\text{s.t.} \quad & \text{Local prediction model (18) with (21)} \\
& \text{Local equality constraints (20) with (21)} \\
& \boldsymbol{u}_{i,k+t|t} \in \boldsymbol{\mathcal{U}_i}, \quad k = 0, 1, \cdots, N-1,
\end{aligned} \tag{23}$$

where w is a positive weighting factor added to introduce a new term in the local cost function to address the agreement protocol. In particular, the agreement term penalizes the difference between the local predicted values of $\lambda_{i,k+t|t}$ and the average of the previously computed optimal values $\lambda^{\star}_{i,k+t|t-1}$ and $\lambda^{\star}_{j,k+t|t-1}$ by the local MPCs i and j at time $t-1$. Here, a_{ii} and a_{ij} are the weighting factors for averaging with the property $a_{ii}, a_{ij} \in [0, 1]$ and $a_{ii} + a_{ij} = 1$, where $i \neq j \in \mathcal{I}$. The last two terms in the cost functions will be described shortly. The distributed MPC (23) has two sets of equality constraints arising from a) the local dynamics (18), and b) the holonomic constraint (20) with the assumption (21).

The proposed local MPC for the agent i does not consider the local dynamics of the other agent (i.e., agent j). Instead, motivated by our previous work [91], it uses the Karush–Kuhn–Tucker (KKT) Lagrange multipliers that correspond to the equality constraint arising from the local dynamics of the agent j in the QP j at time $t-1$. This set of *KKT Lagrange multipliers* is denoted by $\beta^{\star}_{j,t-1}$. In addition, $\mathcal{K}_{j,i}$ and $\mathcal{K}_{j,\lambda}$ represent the *sensitivity* (i.e., gradient) of the local dynamics j with respect to the local variables $(\boldsymbol{x}_i(\cdot), \boldsymbol{u}_i(\cdot))$ and $\lambda(\cdot)$, respectively. In particular, $\mathcal{K}_{j,i}$ can be computed in a straightforward manner by taking the gradient of the local interaction terms $\boldsymbol{\Delta}_j$ with respect to $(\boldsymbol{x}_{i,k+t|t}, \boldsymbol{u}_{i,k+t|t})$ over the entire control horizon and stacking the results together, that is,

$$\mathcal{K}_{j,i} := \frac{\partial \operatorname{col}\{\boldsymbol{\Delta}_j(\boldsymbol{x}_{i,k+t|t}, \boldsymbol{u}_{i,k+t|t}) \,|\, k = 0, 1, \cdots, N-1\}}{\partial(\boldsymbol{x}_i(\cdot), \boldsymbol{u}_i(\cdot))}.$$

An analogous approach can be used to compute the sensitivity matrix $\mathcal{K}_{j,\lambda}$. We then add the last two linear terms to the cost function of the local MPC (23). Our previous work [91, Theorem 1] has shown that the inclusion of the KKT Lagrange multipliers $\beta^{\star}_{j,t-1}$ together with the sensitivity matrices $(\mathcal{K}_{j,i}, \mathcal{K}_{j,\lambda})$ in the cost function can result in a set of local KKT conditions that have a similar structure to that of the KKT equations for the centralized problem. Finally, $\boldsymbol{\mathcal{U}}_i$ in (23) represents the local feasibility set for the GRFs (i.e., inputs).

***Remark** 5:* We remark that local MPCs in the proposed structure (23) share their optimal local state trajectory $\boldsymbol{x}^{\star}_i(\cdot)$, local control trajectory $\boldsymbol{u}^{\star}_i(\cdot)$, local estimates of the Lagrange multiplier trajectory $\lambda^{\star}_i(\cdot)$, and the KKT Lagrange multipliers corresponding to the local dynamics in the QP structure $\beta^{\star}_i$ with the other agent and according to the one-step communication delay protocol (see Fig. 3). Finally, the number of decision variables for each local MPC becomes $(13+\frac{3}{2}\, m_u)\, N$.

IV. Distributed Nonlinear Controllers for Full-Order Models

The objective of this section is to present the low-level and distributed nonlinear controllers for the whole-body motion control of each agent. The full-order and floating-base model of the agent i can be described by the Euler-Lagrange equations and principle of virtual work as follows:

$$\begin{aligned}
D(q_i)\, \ddot{q}_i + H(q_i, \dot{q}_i) = \Upsilon\, \tau_i + \sum_{\ell \in \mathcal{C}_i} J^{\top}_{\ell}(q_i)\, f^{\ell}_i \\
+ J^{\top}_{\text{int}}(q_i)\, (p_i - p_j)\, \lambda,
\end{aligned} \tag{24}$$

where $q_i \in \mathcal{Q} \subset \mathbb{R}^{n_q}$ represents the generalized coordinates of the robot i, $\mathcal{Q}$ and n_q denote the configuration space and the number of degrees of freedom (DOFs), respectively, $\tau_i \in \mathcal{T} \subset \mathbb{R}^{n_\tau}$ represents the joint-level torques at the actuated joints, $\mathcal{T}$ is a closed and convex set of admissible torques, and $\mathcal{C}_i$ represents the set of contacting legs with the environment. In addition, f^{ℓ}_i denotes the GRF at the contacting leg $\ell \in \mathcal{C}_i$ of the full-order model for the agent i. We remark that the GRF at the contacting leg $\ell \in \mathcal{C}_i$ of the reduced-order model for the agent i was denoted by u^{ℓ}_i in Section II. This is due to the possible gap between the reduced- and full-order models arising from abstraction (i.e., ignoring legs' dynamics). Moreover, $D(q_i) \in \mathbb{R}^{n_q \times n_q}$ denotes the positive definite mass-inertia matrix, $H(q_i, \dot{q}_i) \in \mathbb{R}^{n_q}$ represents the Coriolis, centrifugal, and gravitational terms, $\Upsilon \in \mathbb{R}^{n_q \times n_\tau}$ is the input distribution matrix, $J_\ell(q_i)$ denotes the contact Jacobian matrix at the leg ℓ, $J_{\text{int}}(q_i)$ represents the Jacobian of the interaction point p_i, and $(p_i - p_j)\, \lambda$ denotes the interaction force between the two agents as described in the reduced-order model of Section II. The local and full-order state variables for the agent i is defined as $z_i := \operatorname{col}(q_i, \dot{q}_i) \in \mathcal{Q} \times \mathbb{R}^{n_q}$. For future purposes, the vector of GRFs for the agent i is shown by $f_i := \operatorname{col}\{f^{\ell}_i \,|\, \ell \in \mathcal{C}_i\}$.

For the whole-body motion control of each agent, we utilize a QP-based nonlinear controller that maps the desired optimal trajectories and GRFs, generated by the high-level MPC, to the full-order model. For this purpose, we consider the following

time-varying and holonomic output functions, referred to as *virtual constraints* [77], to be regulated:

$$y_i(t, z_i) := y_a(q_i) - y_{\text{des}}(t), \tag{25}$$

where $y_a(q_i)$ represents a set of controlled variables and $y_{\text{des}}(t)$ denotes their desired evolution in terms of a time-based phasing variable. In this paper, the controlled variables include the Cartesian coordinates of the robot's COM, the absolute orientation of the robot's body (i.e., Euler angles), and Cartesian coordinates of the swing feet. The desired evolution of the COM position and Euler angles are generated by the MPC. In addition, the desired evolution of the swing feet's coordinates is taken as a Bézier polynomial connecting the current footholds to the upcoming ones, computed based on Raibert's heuristic [90, Eq. (2.4), pp. 46].

We next implement the I-O linearization technique [71] to differentiate the local outputs (25) twice along the full-order dynamics (24) while ignoring the interaction forces between the agents. This results in the following output dynamics

$$\ddot{y}_i = \Phi_\tau(z_i)\,\tau_i + \Phi_f(z_i)\,f_i + \phi(z_i) = -K_P\,y_i - K_D\,\dot{y}_i + \delta_i, \tag{26}$$

where $\Phi_\tau(z_i)$, $\Phi_f(z_i)$, and $\phi(z_i)$ are proper matrices and vectors computed based on I-O linearization and Lie derivatives similar to [1, Appendix A]. Moreover, K_P and K_D are positive definite matrices, and δ_i is a slack variable to be used later for the feasibility of the QP-based nonlinear controller. Unlike the high-level trajectory planner of Section III that takes into account the interaction terms, the low-level nonlinear controller ignores the interaction forces. In particular, our numerical results in Section V suggest that considering holonomic constraints for trajectory planning is crucial for stabilizing cooperative locomotion. However, the optimal trajectories, generated by the high-level MPC, can be robustly mapped to the full-order model without considering the interaction terms at the low level. This reduces the complexity of the distributed and full-order model controllers.

By stacking together the Cartesian coordinates of the stance feet and then differentiating them twice, one can get an additional constraint to express zero acceleration for the stance feet. In particular, we have

$$\ddot{r}_{\text{foot},i} = \Theta_\tau(z_i)\,\tau_i + \Theta_f(z_i)\,f_i + \theta(z_i) = 0, \tag{27}$$

where $r_{\text{foot},i} := \text{col}\{r^\ell_{\text{foot},i} \,|\, \ell \in \mathcal{C}_i\}$ is a vector containing the Cartesian coordinates of the stance feet for the agent i. Moreover, $\Theta_\tau(z_i)$, $\Theta_f(z_i)$, and $\theta(z_i)$ are proper matrices and vectors computed based on I-O linearization. We then employ the following real-time and strictly convex QP [77] to solve for feasible (τ_i, f_i, δ_i) at 1kHz to meet the output dynamics (26) and the contact equation (27)

$$\begin{aligned}
\min_{(\tau_i, f_i, \delta_i)} \ & \frac{\gamma_1}{2}\|\tau_i\|^2 + \frac{\gamma_2}{2}\|f_i - f_{\text{des},i}\|^2 + \frac{\gamma_3}{2}\|\delta_i\|^2 \\
\text{s.t.} \ & \Phi_\tau(z_i)\,\tau_i + \Phi_f(z_i)\,f_i + \phi(z_i) = -K_P\,y_i - K_D\,\dot{y}_i + \delta_i \\
& \Theta_\tau(z_i)\,\tau_i + \Theta_f(z_i)\,f_i + \theta(z_i) = 0 \\
& \tau_i \in \mathcal{T}, \quad f_i^\ell \in \mathcal{FC}, \quad \forall \ell \in \mathcal{C}_i,
\end{aligned} \tag{28}$$

where γ_1, γ_2, and γ_3 are positive weighting factors, and $f_{\text{des},i}$ represents the desired evolution of the GRFs generated by the high-level MPC. Here we note that the equality constraints, specifically (26) and (27), serve to constrain the formulated QP along the full-order dynamics (24). More specifically, (26) is derived by employing the I-O linearization technique [71] for the virtual constraints (25) and the full-order dynamics (24). Analogous to the derivation of (26), (27) is derived from the non-slippage constraint on each stance foot. Given that the full-order dynamics are embedded within (28) as constraints, the optimal solution adheres to the full-order dynamics. As mentioned in Remark 3, $f_{\text{des},i}$ is identical to the first element of the optimal GRFs, $\boldsymbol{u}^\star_{t|t}$, computed by (16) or (23). The cost function of (28) tries to minimize the effect of the slack variable δ_i in the output dynamics (26) via a high weighting factor γ_3 while 1) imposing the actual GRFs of the full-order model f_i to follow the prescribed force profile $f_{\text{des},i}$ with the weighting factor γ_2, and 2) having the minimum-power torques with the weighting factor γ_1.

Remark 6: We remark that the joint-level torque controller (28) is indeed a nonlinear whole-body control law in terms of the state variables z_i. In particular, the QP-based virtual constraint controller applies the I-O linearization technique to guarantee position tracking while also addressing the friction cone conditions, holonomic constraints, and force tracking. We employ virtual constraint controllers as our previous work has shown that these QP-based nonlinear controllers result in continuously differentiable feedback laws that robustly stabilize gaits for closed-loop systems [77, Theorems 1 and 2]. Furthermore, virtual constraint controllers can systematically address potential underactuation in legged locomotion [58].

V. Numerical and Experimental Validations

This section aims to validate the proposed layered control architecture via extensive numerical simulations and experiments. We study both the reduced- and full-order models of cooperative locomotion in numerical simulations to show the robust stability of the collaborative gaits. We further experimentally investigate the robustness of the trajectories with a team of two holonomically constrained A1 robots, as shown in Fig. 1.

A. Closed-Loop System

1) ***Robot hardware and gait:*** The hardware platform considered here, the A1 robot, is a torque-controlled quadrupedal robot platform with 18 DOFs and 12 actuators. More specifically, 12 DOFs of the system represent the actuated DOFs of the legs' joints. Each leg consists of a 2-DOF hip joint (roll and pitch) and a 1-DOF knee joint (knee pitch). The remaining 6 DOFs describe the unactuated position and orientation of the body with respect to the inertial world frame. The robot is approximately 12.45 (kg) and stands up to about 0.3 (m) off the ground. This work considers a standing height of 0.26 (m) for all experiments. Here, the position of the interaction points with respect to COMs in the body frames $\{B_i\}$ is taken as $d_i^{B_i} = \text{col}(0, 0, 0.15)$ (m) for all $i \in \mathcal{I}$ (see (1)). Different mechanisms are designed to holonomically constrain the motion of two robots with ball joints and an adjustable bar length between the agents (see Fig. 5). Furthermore, the

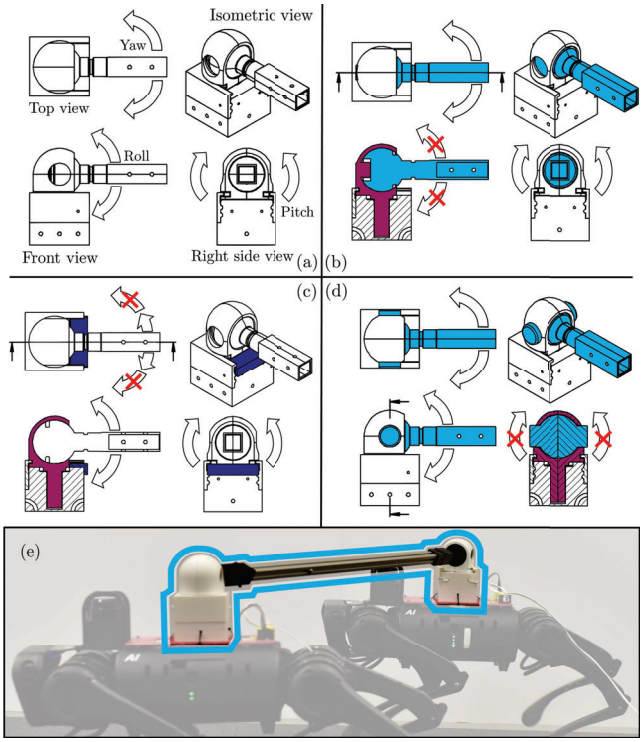

Fig. 5. Illustration of the mechanisms designed to be mounted on the torso of each robot to holonimcally constrain the motion of agents. The mechanism in (a) can implement the holonomic constraint in (2) with free ball joints. The mechanisms in (b), (c), and (d) implement the constraint (2) while also restricting the roll, yaw, and pitch motions, respectively. The mechanism implemented on top of the robots is illustrated in (e).

mechanisms can limit the ball joints to add further constraints on their Euler angles. For numerical and experimental studies in Sections V-B and V-C, the nominal length of the bar is 1 (m) (see Fig. 1). In the following sections, we study a cooperative trot gait with a swing time of 0.2 (s) and at different speeds up to 0.5 (m/s) and subject to external disturbances, uncertainties in holonomic constraints, unknown payloads up to 55% uncertainty in one robot's mass, and on different terrains (e.g., slippery surfaces, wooden blocks, gravel, mulch, and grass).

*2) **Computation, control loop, and network**:* We use RaiSim [92] to simulate both the interconnected reduced- and full-order models numerically. The proposed high-level centralized and distributed MPC algorithms for trajectory planning and the low-level distributed nonlinear controllers for whole-body motion control are solved using qpSWIFT [93] at 200 Hz and 1 kHz, respectively. A joystick is used to command the desired velocity trajectories to the high-level trajectory planner. The joystick includes two 2-DOFs gimbals, six auxiliary switches, and two knobs for the controlling purpose (see Fig. 6). The gimbals are used to generate the desired speed, and the switches are employed to choose if both agents are being controlled simultaneously or if each agent is being controlled individually with different desired speeds. We usually command the same desired speed on both agents. For the purpose of changing the relative positions of the agents, the switches help to change the command mode to send different desired speeds for each agent. Moreover, we remark that the joystick commands the desired trajectories for

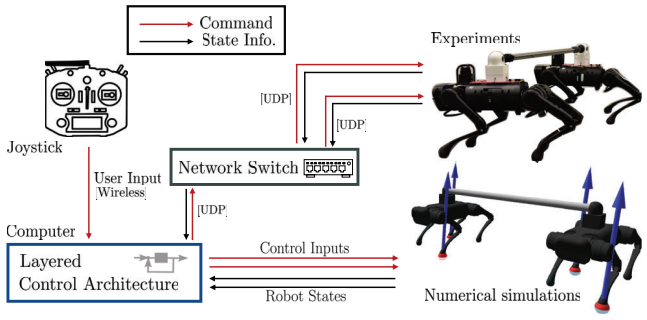

Fig. 6. Numerical and experimental validation system setup. Here, the joystick commands the desired velocity trajectories to the trajectory planner of each agent. Both agents are controlled by one joystick. Joystick sends out the desired trajectories on both numerical simulations and experimental validations. The network switch is used to build the connection between the computer and two agents without IP address collision. UDP communication protocol through Ethernet cables is used in experimental validations.

both the numerical simulations and experimental validations. The joystick connects with the computer through a 2.4 GHz wireless channel as described in Fig. 6.

The proposed layered controller, including the MPC-based trajectory planners and distributed nonlinear controllers, is solved on an off-board laptop computer with an i7-10750H CPU running at 2.60 GHz and 16 GB RAM. All computations in the layered controller are performed on the same laptop computer due to the hardware limitation of the embedded onboard computer on each agent. For the experiment, we use a network switch in the connection between the robotic team and the computer. The connection diagram is illustrated in Fig. 6. The switch supports 1000 Mbps gigabit Ethernet with five ports. The robot IP addresses are redefined to avoid IP collision during communication. Here, we also define the IP routing table and proper IP address on the computer to communicate with both agents without data packet confusion. Internally, a UDP protocol through Ethernet cables is used to communicate between the computer and the robots.

*3) **Tuning controllers**:* The control horizon for both the centralized and distributed MPC is taken as $N = 5$ discrete-time samples, where the time discretization at the high level is 5 (ms). More specifically, the total control horizon length adopted in numerical and experimental validations is 25 (ms). The centralized and distributed MPC algorithms in (16) and (23) have 245 and 125 decision variables, respectively. The control horizon can be larger until the computational cost is no longer within the hardware limitations. Here we note that the adopted control horizon and the number of decision variables are among the tuned parameters that allow stable cooperative locomotion subject to various disturbances and uneven terrains by the proposed MPC. In addition, it has been observed that $N = 5$ is the minimum control horizon to stabilize the MPC. The stage cost gain of the centralized MPC is tuned as $\boldsymbol{Q} = \text{diag}\{Q_{rc1}\ Q_{rc2}\ Q_{\dot{r}c1}\ Q_{\dot{r}c2}\ Q_{\xi 1}\ Q_{\xi 2}\ Q_{\omega 1}\ Q_{\omega 2}\} \in \mathbb{R}^{24\times 24}$, where $\boldsymbol{Q}_{rci} = 10^5 \times \text{diag}\{3\ 300\ 30\}$, $\boldsymbol{Q}_{\dot{r}ci} = 10^4\, \mathbb{I}_{3\times 3}$, $\boldsymbol{Q}_{\xi i} = 10^8\, \mathbb{I}_{3\times 3}$, and $\boldsymbol{Q}_{\omega i} = 5 \times 10^3\, \mathbb{I}_{3\times 3}$, $i \in \mathcal{I}$. The terminal cost gain of the centralized MPC is also tuned as $\boldsymbol{P} = 10^{-1}\boldsymbol{Q} \in \mathbb{R}^{24\times 24}$. The input gains of the centralized MPC are chosen as $\boldsymbol{R}_u = 10^{-2}\, \mathbb{I}_{24\times 24}$ and $\boldsymbol{R}_\lambda = 10^4$. In a similar manner, the stage cost gain and terminal cost gain of the distributed MPC on the i-th agent are tuned as $\boldsymbol{Q}_i =$

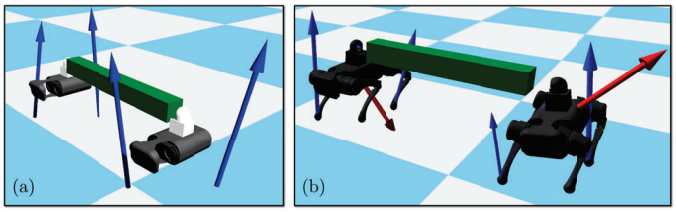

Fig. 7. Snapshots demonstrating the performance of the proposed control approach in numerical simulations. The left figure shows the snapshot of the simulation with the interconnected reduced-order model (torso dynamics) and subject to a 5 (kg) payload (40% uncertainty in one robot's mass) between the agents. The right figure shows the snapshot of the simulation with the full-order model and subject to a 5 (kg) payload between agents and unknown time-varying external disturbances applied to the robots. Arrows at the leg ends describe the GRFs, and the ones on the torso represent the external disturbance forces. The payload is illustrated with a box.

$\text{diag}\{Q_{rci}\ Q_{\dot{r}ci}\ Q_{\xi i}\ Q_{\omega i}\} \in \mathbb{R}^{12\times12}$ and $\boldsymbol{P}_i = 10^{-1}\boldsymbol{Q}_i \in \mathbb{R}^{12\times12}$. The input gains of the distributed MPC are finally chosen as $\boldsymbol{R}_u = 10^{-2}\,\mathbb{I}_{12\times12}$ and $\boldsymbol{R}_\lambda = 10^4$. Additionally, we choose the weighting factor for the agreement protocol in (23) as $w = 10$, and the averaging factors in (23) are chosen as $a_{ii} = a_{ij} = 0.5$ for all $i \neq j \in \mathcal{I}$. The friction coefficient for both the centralized and distributed MPC algorithms is assumed to be $\mu = 0.6$. However, the experiments on slippery surfaces assume a lower friction coefficient of $\mu = 0.3$. For the low-level and distributed nonlinear controllers in (28), the weighting factors for the joint-level torques, force tracking error, and slack variables are chosen as $\gamma_1 = 10^2$, $\gamma_2 = 10^4$, and $\gamma_3 = 10^6$, respectively. We finally remark that the low-level controller uses the same friction coefficient values as the high-level MPC.

The computation time of the centralized and distributed MPC algorithms under nominal conditions (during the steady-state gait on the flat ground) is approximately 1.38 (ms) and 0.41 (ms), respectively. This shows that the solve time with the proposed distributed MPC is reduced by 70% under nominal conditions. We note that the observed difference is similar across the demonstrated scenarios, given that all computations yielded feasible solutions. Furthermore, the computation time of the low-level nonlinear controllers is about 0.12 (ms).

B. Numerical Validation

1) ***Simulation with the reduced-order model****:* We model the interconnected SRB dynamics in the RaiSim environment for numerical validation and apply the optimal GRFs generated from the proposed centralized (16) and distributed MPC (23) algorithms. In particular, the optimal GRFs are applied on each SRB model with the position offset from each body center. Here, the position offset represents the foothold position. In Fig. 7(a), the arrows represent the optimal GRFs, and the origins of the arrows are the offset positions where the optimal GRFs are applied to each SRB model. In addition, for comparison purposes, we apply the GRFs generated from the nominal MPC that considers a standard SRB model *without* the holonomic constraints to this interconnected model. More specifically, the formulation of the nominal MPC can be achieved by removing the reference to the Lagrange multiplier, λ, in (16) and without (15). Due to the elimination of the portion representing the interaction forces and holonomic constraints, the optimal GRFs generated from the nominal MPC have no consideration of the interconnection between agents. The evolution of the desired and actual COM velocities using the nominal MPC is depicted in Fig. 8(a). In the simulation with the nominal MPC, we only apply the holonomic constraint to the robots and without any payloads and monitor the behavior of the system. The plot shows that the nominal MPC *cannot* stabilize the interconnected reduced-order system. On the other hand, the interconnected SRB model performs robustly stable cooperative locomotion when integrated with the GRFs generated from the proposed centralized and distributed MPCs, as shown in Figs. 8 (b) and (c), respectively. In these simulations, an unknown payload of 5 (kg) (40% uncertainty in one robot's mass) is considered between the agents (i.e., in the middle of the bar), and the joystick provides the desired trajectories. Animations of all simulations can be found online [94].

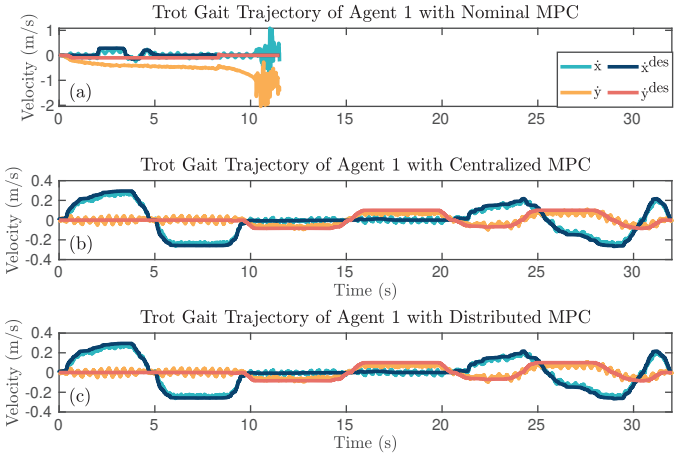

Fig. 8. Plots of the desired and actual velocities of the closed-loop interconnected reduced-order model for two agents in the numerical simulation. Here, the optimal GRFs are generated by the (a) nominal MPCs, (b) centralized MPC (16), and (c) distributed MPCs (23) and are applied to the reduced-order models. An unknown payload of 5 (kg) between agents is applied to the reduced-order models in (b) and (c) to show tracking performance subject to unknown disturbances.

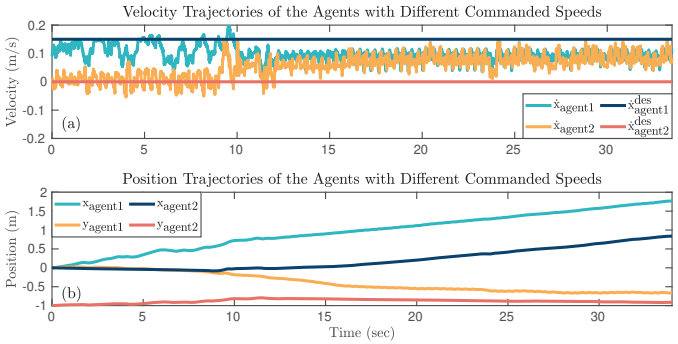

Fig. 9. (a) Plots of the desired and actual velocities of the closed-loop interconnected reduced-order model when the desired velocities are not identical. (b) Plots of the actual COM positions of two agents. The commanded velocity on the first and second agents is taken as 0.15 (m/s) and 0 (m/s), respectively. Here, the optimal GRFs are generated by the distributed MPCs (23).

If the commanded desired velocities to the agents are not equal, the constraint (7) may be violated for the desired trajectory profiles. In this case, the distributed MPCs may compute optimal trajectories close to the commanded ones that meet the holonomic constraints (2), (7), and (10). To illustrate this, we command the desired forward speeds of 0.15 (m/s) and 0 (m/s) to the first and second agents, respectively. Figure 9(a)

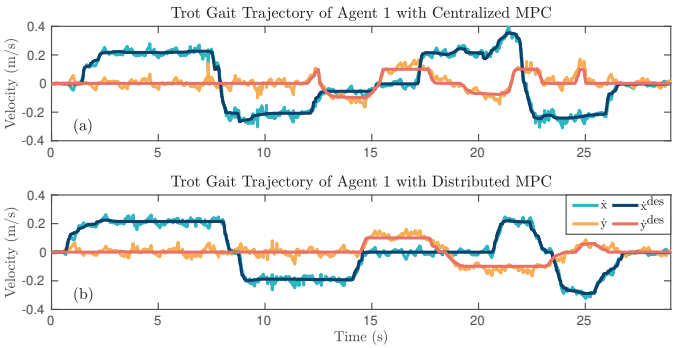

Fig. 10. Comparison between the desired velocities and optimal velocities, generated with the high-level centralized and distributed MPCs, for the closed-loop interconnected full-order model in RaiSim. The figure depicts the optimal trajectories generated by (a) the centralized MPC (16) and (b) the distributed MPC (23) for agent 1. Here, we consider a trot gait over rough terrain with an unknown payload of 5 (kg) between the agents and subject to unknown, time-varying, and external disturbance forces applied to the robots.

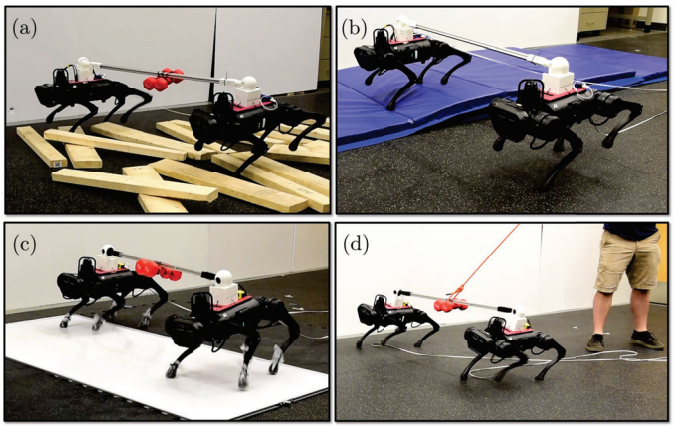

Fig. 11. Snapshots demonstrating the performance of the proposed layered control algorithm for a series of cooperative locomotion experiments. Indoor experiments: (a) rough terrain with the agents traversing arbitrarily displaced wooden blocks, (b) asymmetrical terrain with one agent being on a compliant surface and elevated by 10 (cm), (c) slippery surface covered by a cooking spray, and (d) tethered pulling. The robots are loaded with a payload of 4.53 (kg) (36% uncertainty in one robot's mass) in (a), (c), and (d). The friction coefficient is taken as $\mu = 0.3$ in (c) and $\mu = 0.6$ in (a), (b), and (d). Here, (a) and (b) show the snapshots where the centralized MPC is applied, while (c) and (d) show the snapshots where the distributed MPC is employed.

depicts the closed-loop velocity trajectories of two agents that meet the holonomic constraint (7). The closed-loop position trajectories of the two agents are also shown in Fig. 9(b), where the coordination of agents is changed compared to Fig. 8, and one agent follows the other. In addition, we remark that the distributed MPCs for the simulation of Fig. 9 do not show any infeasibility.

*2) **Simulation with the full-order model**:* We next numerically study the performance of the closed-loop system with the interconnected full-order dynamical model in RaiSim. Here, the proposed layered control approach is employed, including the centralized and distributed MPC algorithms for trajectory planning and nonlinear controllers for whole-body motion control. The desired time-varying trajectories are generated using the joystick. The high-level MPC then generates optimal GRFs and reduced-order trajectories. The distributed low-level controller computes the corresponding joint-level torques to impose the full-order model to track the optimal trajectories. An overview of the numerical simulation environment for the full-order model is illustrated in Fig. 7(b). The desired

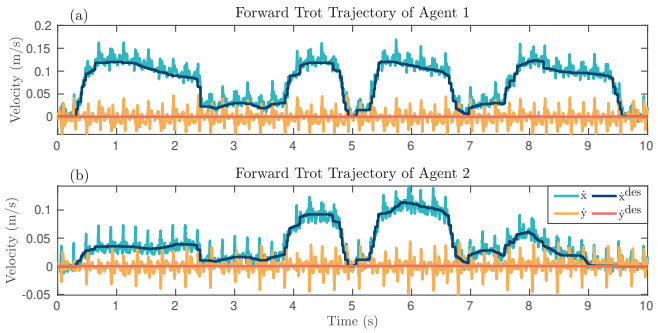

Fig. 12. Comparison between the desired and optimal velocities of the robots for the nominal trot experiment on flat ground. Optimal velocities are provided from the high-level centralized MPC. Time-varying desired trajectories are provided by the joystick to coordinate the robots' motions. The centralized MPC's outputs track the desired trajectories.

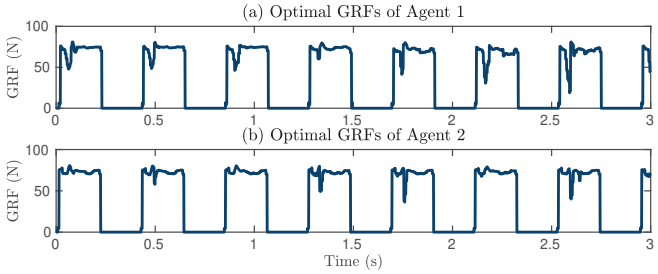

Fig. 13. Plots of the optimal GRFs generated from the centralized MPC during the nominal trot experiment on flat ground. The figure depicts the z components of the optimal GRFs for the left front leg of each agent.

trajectories provided by the joystick, together with the optimal trajectories computed by the centralized and distributed MPC, are depicted in Figs. 10(a) and 10(b). Due to the similarity of the plots for agents, Fig. 10 only includes the trajectories for agent 1. Here, we consider the trot gait over a randomly generated rough terrain with a maximum height of 5 (cm) (19% uncertainty in the robot's nominal height). The gait is also subject to an unknown payload of 5 (kg) and an unknown sinusoidal external disturbance force with a magnitude of 20 (N) and the period of 1.0 (s), 0.7 (s), and 0.4 (s) along the x-, y-, and z-directions, respectively. The simulation results show that the closed-loop system robustly tracks the desired trajectories.

C. Experimental Validation and Robustness Analysis

This section experimentally validates the proposed layered control approach with the high-level centralized and distributed MPC algorithms and the low-level distributed nonlinear controllers.

*1) **Indoor experiments with the centralized MPC**:* In the indoor experiments, we employ the proposed layered control algorithm on two A1 robots subject to holonomic constraints, where ball joints are applied at the interaction points (see Fig. 11). We first investigate the nominal and cooperative trot gait with the centralized MPC algorithm on flat ground and without disturbances. The desired and optimal COM trajectories, generated by the high-level MPC, together with the generated optimal GRFs, are illustrated in Fig. 12 and Fig. 13, respectively. The plots show that the team of two A1 robots performs stable cooperative locomotion while the trajectory planner effectively tracks the time-varying desired trajectories. Furthermore, the optimal GRFs generated by the centralized

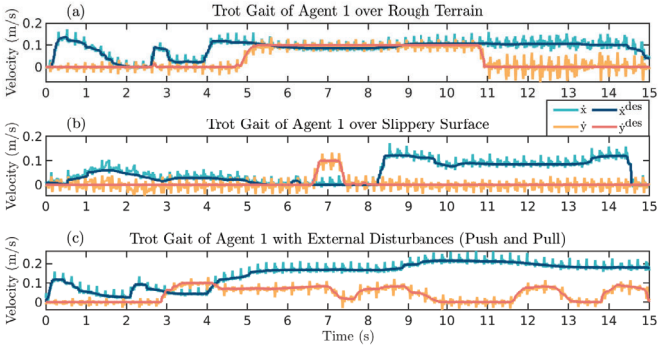

Fig. 14. Plots of the desired and optimal velocities for cooperative locomotion experiments on (a) rough terrain, (b) a slippery surface, and (c) subject to external disturbances with the centralized MPC. The plots show that the centralized MPC's outputs can robustly track the desired trajectories in the presence of uncertainties and disturbances.

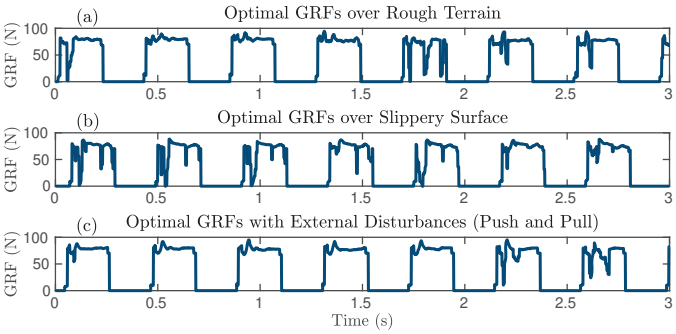

Fig. 15. Plots of the optimal GRFs, generated by the centralized MPC, for cooperative locomotion experiments on (a) rough terrain, (b) a slippery surface, and (c) subject to external disturbances. The figure depicts the optimal GRFs for the left front leg of agent 1 along the z-direction.

MPC are feasible, with the vertical component value being close to 60 (N), which is approximately the force required by each stance leg to support the total mass of each robot during trotting.

We further investigate the robustness of the proposed layered control approach by studying the tracking performance of the closed-loop system with different experiments, including locomotion on rough terrain (see Fig. 11(a)), locomotion on a slippery surface (see Fig. 11(c)), and locomotion subject to unknown external disturbances (see Fig. 11(d)), as shown in Figs. 14(a), 14(b), and 14(c), respectively. In these experiments, the rough terrain is made of randomly displaced wooden blocks with a maximum height of 5 (cm) (19% of the robot's height). Moreover, the slippery surface is a whiteboard covered with cooking spray. The unknown external disturbances are further applied by a human user, including pushes and tethered pulls on both agents. The robots cooperatively transport an unknown payload of 4.53 (kg) (36% uncertainty in one robot's mass) in all these experiments. The optimal GRFs computed by the MPC on rough terrain, on the slippery surface, and subject to external disturbances are depicted in Figs. 15(a), 15(b), and 15(c), respectively. We remark that despite the uncertainties, the GRFs are in the feasible range, and the MPC's outputs robustly track the desired and time-varying trajectories. Furthermore, the phase portraits of the body's roll and pitch motions (i.e., unactuated DOFs) during these cooperative trot gaits are shown in Figs. 16(a) and 16(b).

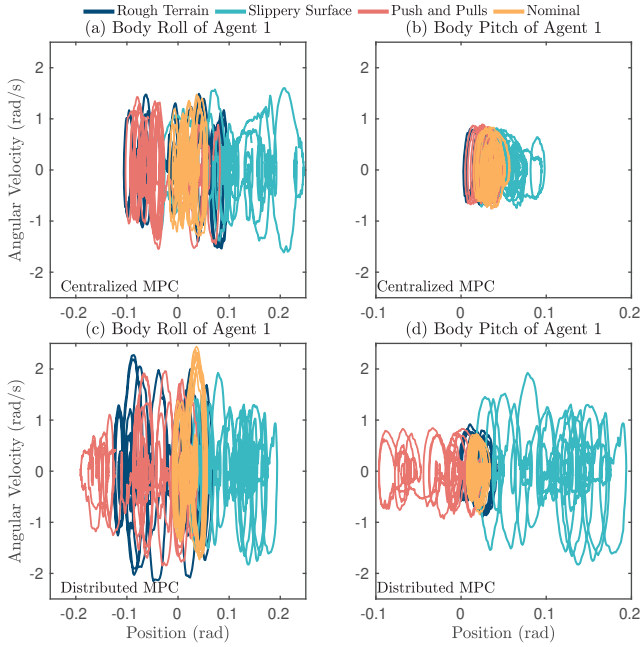

Fig. 16. Phase portraits for (a) the body roll and (b) the body pitch of agent 1 with the centralized MPC and (c) the body roll and (d) the body pitch of agent 1 with the distributed MPCs during different experiments. The plots show the robustness of the cooperative locomotion over rough terrain covered with randomly dispersed wooden blocks, the slippery surface, and subject to unknown external disturbances.

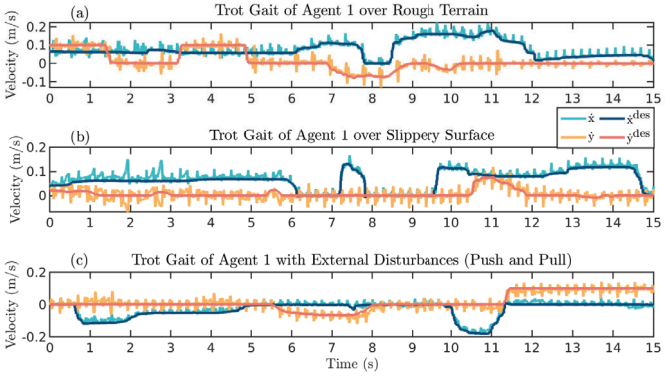

Fig. 17. Plots of the desired and optimal velocities for cooperative locomotion experiments on (a) rough terrain, (b) a slippery surface, and (c) subject to external disturbances with the distributed MPC. The plots show that the distributed MPC's outputs can robustly track the desired trajectories in the presence of uncertainties and disturbances.

Figure 16 indicates that the evolution of the robots' states is bounded during the cooperative gaits in the presence of various unknown terrains and disturbances, which in turn implies robust stability of the gait. Videos of all experiments are available online [94].

*2) **Indoor experiments with the distributed MPC**:* In this part, we evaluate the performance of the closed-loop system with the proposed distributed MPC algorithm in similar indoor experiments (see Fig. 11). The evolution of the optimal trajectories generated from the distributed MPC and time-varying desired trajectories during the cooperative transportation of the same payload over rough terrain, the slippery surface, and subject to unknown disturbances is illustrated in Figs. 17(a), 17(b), and 17(c), respectively. The optimal GRFs are also shown in Fig. 18. The phase portraits of the body's roll and pitch motions during the cooperative gait with the

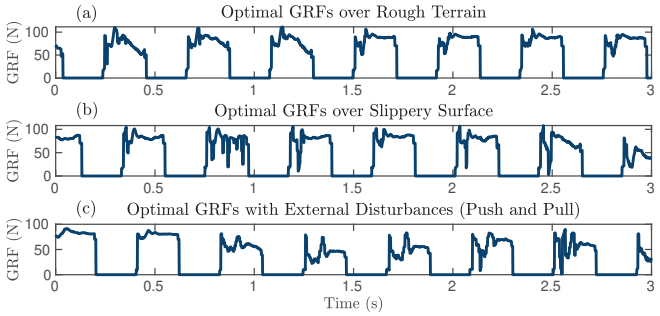

Fig. 18. Plots of the optimal GRFs, generated by the distributed MPC, for cooperative locomotion experiments on (a) rough terrain, (b) a slippery surface, and (c) subject to external disturbances. The figure depicts the optimal GRFs for the left front leg of agent 1 along the z-direction.

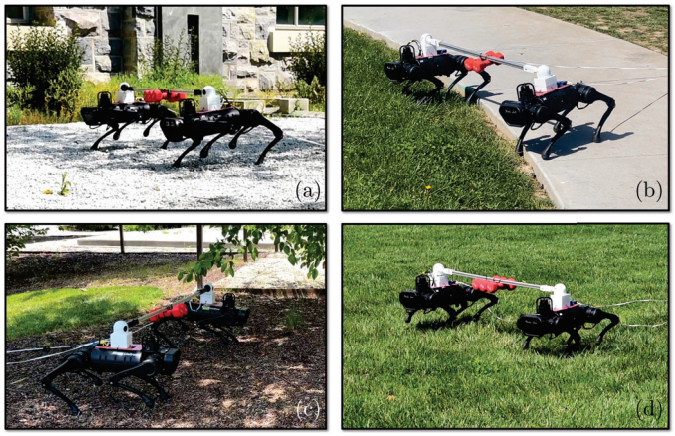

Fig. 19. Snapshots demonstrate the proposed layered controller's performance for a series of cooperative locomotion experiments. Outdoor experiments: (a) cooperative locomotion on gravel, (b) transitioning from concrete surface to grass, (c) cooperative locomotion on mulch, and (d) cooperative locomotion on grass. The robots cooperatively transport a payload of 4.53 (kg) (36% uncertainty) in (b) and (c) and 6.80 (kg) (55% uncertainty) in (a) and (d). Here, (a) and (c) show the snapshots where the distributed MPC is adopted, while (b) and (d) show the snapshots where the centralized MPC is employed.

distributed MPC algorithm and subject to these uncertainties are depicted in Figs. 16(c) and 16(d). We observe that the optimal GRFs, generated by the MPC, remain feasible, and the MPC's outputs robustly track the desired trajectories in the presence of unknown terrains and external disturbances.

*3) **Outdoor experiments with centralized and distributed MPCs**:* We next investigate the performance and robustness of the closed-loop system with the centralized and distributed MPC algorithms in different outdoor experiments, as shown in Fig. 19. These experiments include cooperative locomotion on gravel, concrete, mulch, and grass subject to unknown payloads. In these studies, we investigate two different payloads: a payload of 4.53 (kg) (36% uncertainty) in Figs. 19(b) and 19(c) and a payload of 6.80 (kg) (55% uncertainty) in Figs. 19(a) and 19(d). The evolution of the virtual constraints (25) for trotting over the gravel and transitioning from concrete to grass with the centralized MPC and trotting over mulch and grass with the distributed MPC is shown in Fig. 20. As the virtual constraint plots stay close to zero, we can conclude that the full-order system effectively tracks the optimal reduced-order trajectories generated by the high-level MPCs. We observe that the proposed layered control approach with both centralized and distributed MPCs can robustly stabilize cooperative gaits in the presence of payloads on unknown outdoor terrains.

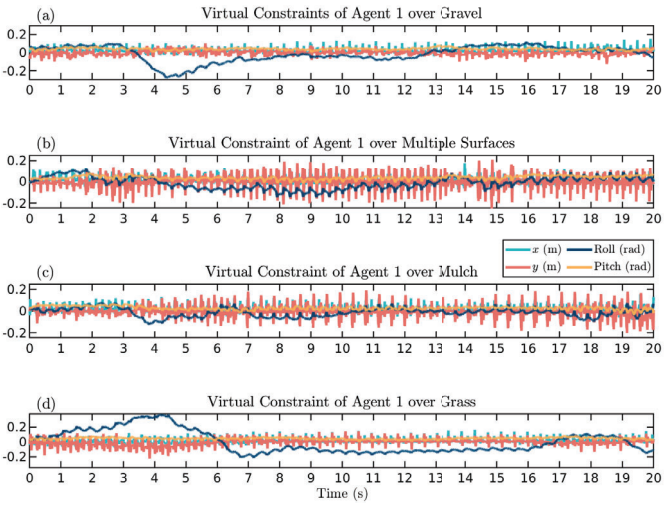

Fig. 20. Plots of the virtual constraints of agent 1 during cooperative locomotion with unknown payloads and on various outdoor terrains, including (a) locomotion on gravel, (b) transitioning from concrete to grass, (c) locomotion on mulch, and (d) locomotion on grass. The payload is 4.53 (kg) in (b) and (c) and 6.80 (kg) in (a) and (d). Here, (a) and (c) depict the evolution of virtual constraints with the distributed MPC at the high level. In addition, (b) and (d) illustrate the evolution of the virtual constraints with the centralized MPC at the high level. Here, we plot the components of virtual constraints in (25) that correspond to the COM position along the x and y axes (m) (i.e., COM position tracking) and the body's roll and pitch angles (rad) (i.e., angle tracking). The plots show that the full-order system tracks the prescribed optimal and reduced-order trajectories generated by the MPCs.

VI. Discussion and Comparison

Numerical simulations and experimental validations in Section V show the effectiveness of the proposed centralized and distributed MPC algorithms for cooperative locomotion. This section aims to analyze and compare the performance of the proposed MPCs while discussing their limitations.

A. Comparison of the Centralized and Distributed MPCs

The robustness of the cooperative locomotion with the proposed centralized and distributed MPC algorithms in the presence of various uncertainties and disturbances is studied numerically and experimentally in Section V. To compare the performance and robustness of the proposed trajectory planners, we apply the nominal, centralized, and distributed MPCs over 1500 randomly generated rough terrains in the simulation environment of RaiSim, as shown in Fig. 21(a). Here, the randomly generated landscapes' maximum height is 12 (cm) (46% uncertainty in the robot's height). Furthermore, the total length of the terrain is assumed to be 10 (m). In these simulations, we evaluate the cooperative locomotion as a success if the agents reach 10 (m) without losing stability. We assess the locomotion as a failure if at least one of the agents' bodies touches the ground before reaching 10 (m). The success rate versus the length of the terrain is depicted in Fig. 21(b). The overall success rate of the nominal, centralized, and distributed MPCs is 0%, 54.2%, and 53.8%, respectively.

Similarly, we compare the performance and robustness of the nominal, centralized, and distributed MPCs subject to 1200 randomly generated external forces and payloads, as shown in Fig. 21(c). The external force is taken as sinusoidal with a maximum amplitude of 80 (N) (65% of one robot's weight) and a maximum period of 4 (s) on the x-, y-, and z-directions.

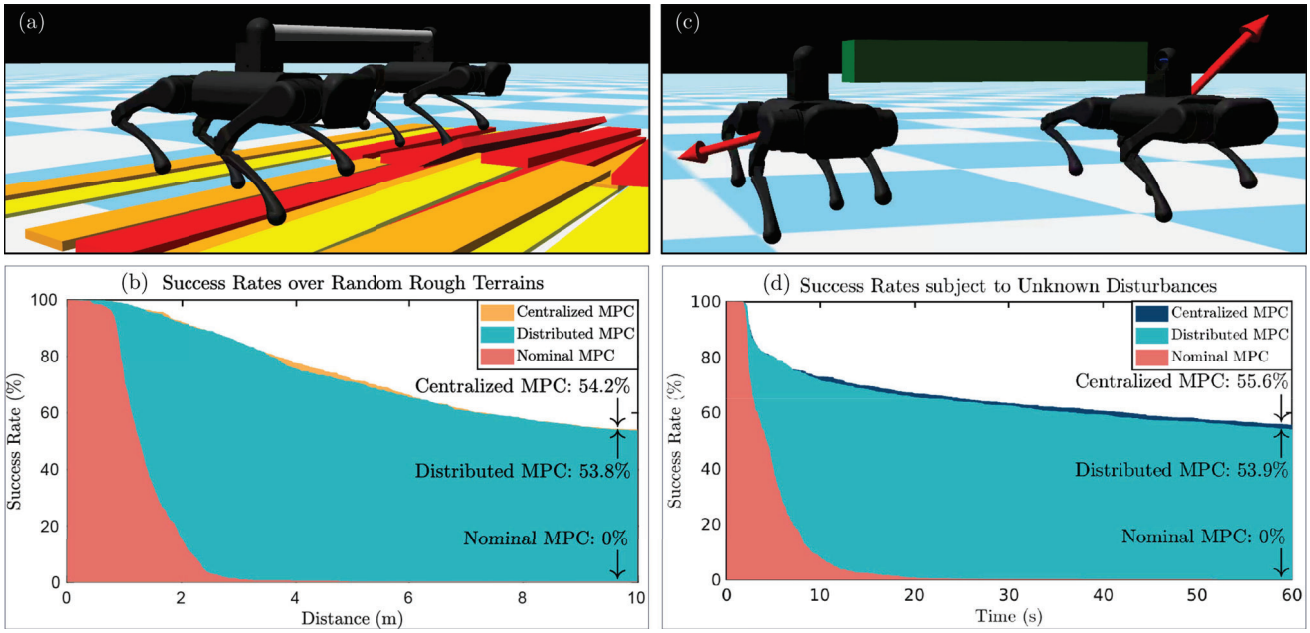

Fig. 21. Illustration of the comparison results between the nominal, centralized, and distributed MPCs. (a) The snapshot shows the RaiSim simulation environment with one of the randomly generated rough terrains. The maximum height of the generated terrains is 12 (cm) (46% uncertainty in robots' height). (b) The plot describes the success rate of the proposed trajectory planners over 1500 randomly generated rough terrains in simulations. The overall success rate of the nominal, centralized, and distributed MPCs over randomly generated rough terrain is 0%, 54.2%, and 53.8%, respectively. (c) The snapshot shows the RaiSim simulation environment with one of the randomly generated external forces and a randomly generated payload. The arrows illustrate the applied external forces on each agent. The maximum external force is 80 (N) (65% of one robot's weight) on the x-, y-, and z-directions. The evolution of the forces in each direction is sinusoidal, with a maximum random period of 4 (s). External forces are applied from 1 (s) to 60 (s). The maximum payload mass is 5 (kg). (d) The plot describes the success rate of the trajectory planners with 1200 randomly applied external forces and payloads in numerical simulations. The overall success rate of the nominal, centralized, and distributed MPCs subject to external forces and payloads is 0%, 55.6%, and 53.9%, respectively.

The maximum mass of the payload is also assumed to be 5 (kg). We evaluate the cooperative locomotion as a success if the agents sustain the stability until 60 seconds. We assess the locomotion as a failure if at least one of the agents' bodies touches the ground before 60 (s). The success rate versus time is depicted in Fig. 21(d). The overall success rate of the nominal, centralized, and distributed MPCs is 0%, 55.6%, and 53.9%, respectively.

Our experimental studies in Figs. 12-18 and Fig. 20 suggest that the proposed centralized and distributed trajectory planners show similar robustness in indoor and outdoor experiments. Slightly better robustness has been observed in numerical simulations of Fig. 21 when employing the centralized MPC at the high level. Still, the success rate between the centralized and distributed MPCs does not significantly differ. These comparisons suggest that the proposed centralized and distributed MPCs can robustly stabilize dynamic cooperative locomotion. We observe that the distributed MPC has less computation time in numerical and experimental studies. However, it is essential to note that the computation time of centralized MPC may potentially be reduced with more efficient implementation methods. In addition, the primary advantage of the distributed MPC approach lies in its inherent reliability. Specifically, instead of relying on centralized decision-making, the distributed MPC approach enables each agent to act independently, informed by knowledge of the other agent's optimal trajectory derived from the previous solution. The centralized MPC has a straightforward synthesis procedure and assumes that all states from two agents are readily available for decision-making. In case of communication issues or limited computation resources, the distributed MPC can be beneficial as it assumes a one-step communication delay and reduces the computational burden of the planners. However, it has a more complex formulation.

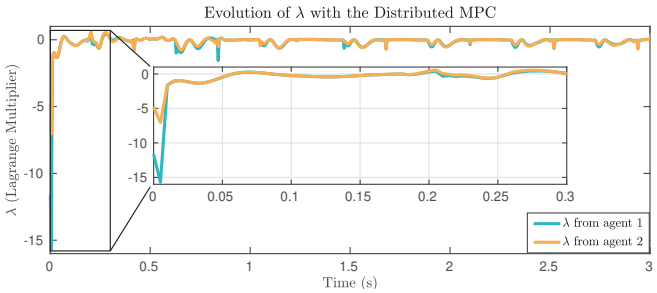

Fig. 22. Plots of the locally estimated Lagrange multipliers $\lambda_{1,t|t}$ and $\lambda_{2,t|t}$ by two agents using the distributed MPC algorithm. The local values reach an agreement and stay close to each other.

B. Evolution of the Lagrange Multiplier in Distributed MPC

Section VI-A demonstrated a similar success rate for the centralized and distributed MPC algorithms with the randomly generated terrains and disturbances. To further study this similar robust stability behavior, Fig. 22 illustrates the evolution of the Lagrange multiplier, λ, computed for each agent with the distributed MPCs. In formulating the distributed MPC, each agent locally computes the Lagrange multiplier according to the one-step communication delay and the agreement protocol. Therefore, λ on each distributed MPC evolves differently. We introduced the consensus protocol in the cost function of (23) to mitigate the divergence of the local estimates and to impose the agreement. The magnified portion of the plot in Fig. 22 shows that the initial λ values on each agent

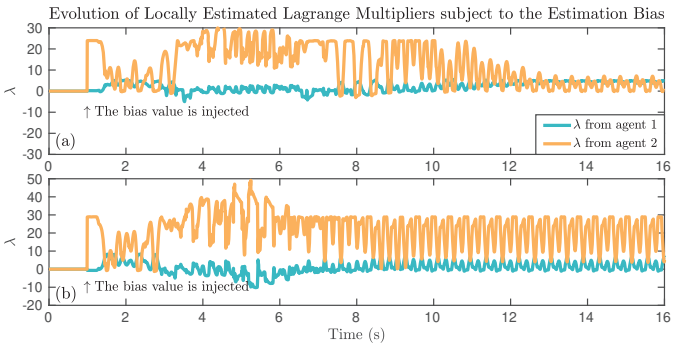

Fig. 23. Plots of the locally computed Lagrange multipliers $\lambda_{1,t|t}$ and $\lambda_{2,t|t}$ using the distributed MPC algorithm subject to a constant estimation bias of (a) 48 (N/m) and (b) 58 (N/m). The bias in estimating the Lagrange multipliers is injected at time 1(s) and continues till the end of simulations. The estimated Lagrange multipliers from local MPCs robustly come to an agreement during the steady state in (a), whereas the agreement does not happen in (b).

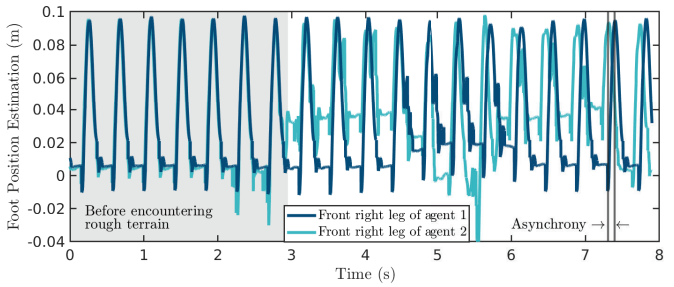

Fig. 24. Plots of the estimated height of agents' front right legs. Initial locomotion has complete synchrony before encountering the rough terrain described in the gray area in the plot. After engaging the rough terrain, asynchrony happens between agents. However, the layered control approach robustly stabilizes the cooperative gait.

are different while converging after a short amount of time according to the consensus protocol. The plot also shows that each agent's λ values are not precisely the same during cooperative locomotion. However, we can observe that both λ values stay close.

To study the robustness of the distributed MPC and consensus protocol, we assume that there is a constant bias in the one-step communication delay for sharing the optimal estimated values of λ between local MPCs. In particular, we suppose that the optimal estimated values computed by the local MPC of agent $j = 1$ (i.e., $\lambda^{\star}_{j,k+t|t-1}$) are used subject to an additive bias amount of 48 (N/m) in the cost function of (23) associated with the local MPC of agent $i = 2$. More specifically, we replace $\lambda^{\star}_{j,k+t|t-1}$ by $\lambda^{\star}_{j,k+t|t-1} + 48$ in the consensus term of the cost function for the local MPC (23) of the agent 2. Furthermore, this bias is assumed to be one-directional in that a similar bias is not considered for the cost function of the local MPC 1. This can help us to study the stability margin in the consensus protocol and estimation. Figure 23(a) depicts the evolution of the local optimal Lagrange values (i.e., $\lambda_{1,t|t}$ and $\lambda_{2,t|t}$) computed by the distributed MPCs versus the time. Here, the bias value of 48 (N/m) is injected at time 1(s). Before this time, the local Lagrange multipliers have almost the same values (i.e., agreement), and after the injection of the bias, there is a transient response. Finally, the local Lagrange multipliers reach the steady-state phase and come to an agreement again (after 13(s)). In this simulation, the robots have stable locomotion. However, their relative positions with respect to each other change over time during the transient

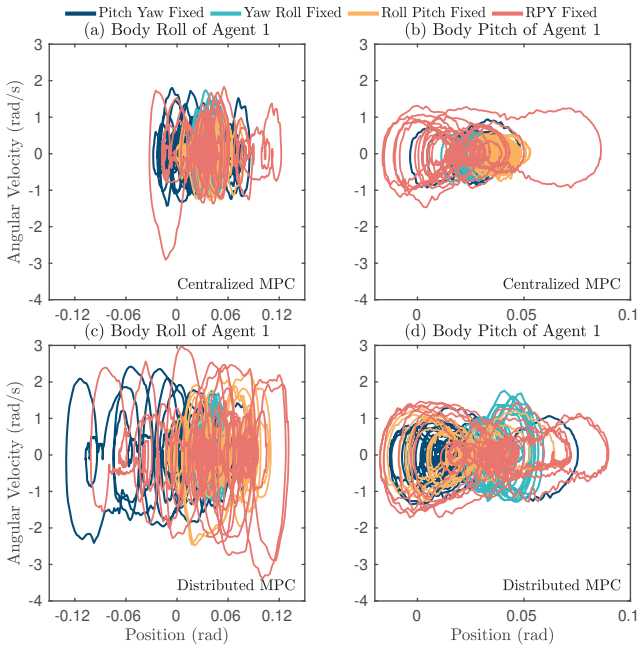

Fig. 25. Phase portraits for (a) the body roll and (b) the body pitch of agent 1 with the centralized MPC and (c) the body roll and (d) the body pitch of agent 1 with the distributed MPC during different experiments. The plots show the robustness of the cooperative locomotion over rough terrain with fixed DOFs in holonomic constraints on the roll, pitch, and yaw directions.

phase, whereas this relative position becomes constant during the steady-state phase. This agreement behavior happens for all bias values less than 48 (N/m). This simulation also confirms the robustness of the distributed controller over an inaccurate estimation of the Lagrange multipliers. Finally, Fig. 23(b) illustrates the evolution of the Lagrange multipliers for a higher value of the bias taken as 58 (N/m). Here, a steady-state phase occurs, but there is no agreement in the local estimations of λ. Furthermore, the relative positions of the agents in this latter simulation change in a periodic manner during the steady-state mode (after 13(s)).

C. Synchronization and Asynchronization

We aim to study the robustness of the layered control approach against possible phase differences between agents that can easily occur on rough terrain, where the discrete-time transitions (i.e., impacts) happen earlier or later than anticipated times on normal gaits. To further investigate this point, we study the estimated height of the agents' front right legs over rough terrain in Fig. 24. Both agents are synchronized at the beginning of the locomotion. After encountering the rough terrain, the asynchrony is observed in Fig. 24. However, the proposed centralized and distributed MPCs show robust cooperative gaits over unknown rough terrains, as shown in Figs. 11(a), 16, 19, and Fig. 20. Moreover, the robustness subject to more than 1000 randomly generated rough terrains is also validated in Fig. 21.

D. Robustness Against Unknown Holonomic Constraints

The holonomic constraint of Section II assumes a distance constraint between the interaction points of agents. In particular, we take no additional rotational constraints at the interaction points. This assumption simplifies the interconnected

SRB model and, thereby, the centralized and distributed MPC algorithms. However, more sophisticated connections could exist, such as limited DOFs on both ends of the holonomic constraint. Here, we study the robustness of the proposed MPCs subject to uncertainties arising from rotational restrictions at the interaction points. These constraints can arise from cooperative loco-manipulation in various applications. Figure 25 depicts the body roll and pitch evolution during cooperative locomotion over rough terrain with different holonomic constraints at the interaction points, including restrictions on ball joints' pitch-yaw, yaw-roll, roll-pitch, and roll-pitch-yaw. These restrictions are implemented with the different mechanisms designed in Fig 5. The robust stability of the cooperative locomotion with the proposed centralized MPC is shown in the phase portraits of the body roll and body pitch in Figs. 25(a) and 25(b). The robust stability of the proposed distributed MPC is also illustrated in Figs. 25(c) and 25(d). We observe that the cooperative locomotion over rough terrain with different and unknown holonomic constraints has robust stability similar to the one illustrated in Fig. 16. However, the phase portraits in Fig. 25 show that the unknown additional interactions from the limited DOFs on both ends of the holonomic constraint can induce aggressive angular positions and velocity changes.

E. Limitations and Future Study

1) ***Feasibility of the MPC****:* There is a possibility of infeasibility when solving the centralized and distributed MPCs since we did not consider adding the slack variables to guarantee feasibility. However, MPCs have not shown infeasibility during numerical simulations and experimental evaluations of Section V. We also remark that the proposed trajectory planners do not show infeasibility in the numerical simulations described in Fig. 9, where the desired velocities are not consistent with the holonomic constraints. More specifically, the proposed trajectory planners generate the optimal GRFs that induce new feasible velocity trajectories that meet the holonomic constraints. Even though the validations in this paper show the feasibility of the MPCs in various scenarios, adding slack variables to the equality constraints of MPCs can relax the conditions arising from the dynamics and holonomic constraints. This can further improve the numerical stability of the trajectory planners.

2) ***Optimal control with switching****:* The proposed MPC approaches for cooperative locomotion were shown to be very robust to various unknown terrains and subject to unknown disturbances. However, the gait presented here does not exhibit extremely dynamic or highly agile maneuvers. One of the reasons for this is the relatively small planning horizon (25 (ms)). While the distributed approach provides an interesting avenue to explore longer horizons in future work due to the considerable decrease in computation time, long horizons suffer when only considering the current domain. For this reason, future work should not only explore increased planning lengths but should also consider a PWA optimal control formulation [88, Chap. 16] such that the change in stance leg configurations can be considered directly by the planner.

3) ***Sophisticated constraints between agents****:* We assumed the holonomic constraint (2) with a ball joint on agents to simplify the development of the interconnected reduced-order model and the synthesis of centralized and distributed MPCs. We further studied the robustness of the proposed layered control approach subject to the unknown restrictions on the ball joints in Section VI-D. However, based on the necessity, the holonomic constraints in (2), (7), and (10) can be generalized to include additional constraints. This will increase the number of Lagrange multipliers, and a modified model, based on (3), can be used to describe the evolution of the system subject to additional constraints. One application can be sophisticated cooperative loco-manipulation for quadrupedal robots.

4) ***Extension to multi-agents****:* Our previous work [1] presented quasi-statically stable cooperative gaits for $M \geq 2$ agents. In particular, a closed-form expression for the interconnected LIP models was developed to address the real-time trajectory planning based on a centralized MPC algorithm. The interconnected LIP model *cannot* address interaction torques between the agents. Furthermore, the gait is *not* dynamic. The current paper presents an interconnected reduced-order model, based on the SRB dynamics, that addresses interaction torques between the agents while allowing dynamic cooperative gaits. However, a closed-form expression for the Jacobian matrices in (13) and (15) may not be easily computed for $M \geq 3$ interconnected SRB dynamics with sophisticated holonomic constraints. Our future work will investigate the extension of the approach for dynamic cooperative locomotion of $M \geq 3$ agents with complex holonomic constraints. One possible way is to develop robust distributed MPC algorithms integrated with reinforcement learning and data-driven techniques [56], [83] to bridge the gap between interconnected reduced-order models and full-order models. Considering the team of constrained two (multiple) legged robots as one unique and complex structure is another possible way for future studies. This will enable us to develop planning and control algorithms for the sophisticated gaits of the whole structure. We will also study the computational burden of these algorithms.

5) ***Coordination between agents****:* In numerical simulations, each agent's global coordinates can be easily used without sensor limitations or unexpected noises. However, experimental evaluations estimate the agents' global coordinates via kinematic estimators. The estimation errors may result in unexpected coordination changes. This paper addresses this issue by the human operator who coordinates the agents with the corresponding speed commands from the joystick. For example, the user commands a higher or lower desired speed to the lagging or leading agent, respectively. Our future work will investigate the design of algorithms that robustly estimate the global coordinates of the agents with noisy measurements.

VII. Conclusion

This paper presented a layered control algorithm for real-time trajectory planning and robust control for cooperative locomotion of two holonomically constrained quadrupedal robots. An innovative reduced-order model of cooperative locomotion is developed and studied based on interconnected SRB dynamics. At the high level of the layered control

algorithm, the real-time trajectory planning problem is formulated as an optimal control problem of the interconnected reduced-order model with two different schemes: centralized and distributed MPCs. The centralized MPC plans for the global reduced-order states, global GRFs, and the interaction wrenches between agents. The distributed MPC assumes the one-step communication delay and an agreement protocol to solve for the local reduced-order states, local GRFs, and the local estimated wrenches. At the low level of the control scheme, distributed nonlinear controllers, based on QP and virtual constraints, are developed to impose the full-order model of each agent to track the optimal reduced-order trajectories and GRFs prescribed by the high-level MPCs.

The effectiveness of the proposed layered control approach was verified with extensive numerical simulations and experiments for the blind and robust cooperative locomotion of two holonomically constrained A1 robots with different payloads on different terrains and subject to external disturbances. A detailed study was presented to compare the performance of the proposed centralized and distributed MPCs over more than 1000 randomly generated landscapes and external pushes. It was shown that the distributed MPC has a robust stability performance similar to that of the centralized MPC, while the computation time is reduced significantly. The results also show that both the centralized and distributed MPCs integrated with the interconnected SRB dynamics can drastically improve the robust stability of cooperative locomotion compared to the individual nominal MPCs. The experimental results suggest that the proposed control algorithm can result in robustly stable cooperative locomotion on different terrains subject to unknown payloads and external disturbances at different speeds. The robustness of the control approach was also studied against uncertainties in holonomic constraints and assumptions. The centralized MPC has a simpler synthesis procedure. However, it assumes ideal communication conditions between the agents, such as the availability of all state variables. Distributed MPC is developed based on a decomposition of the centralized MPC subject to a one-step communication delay and an agreement protocol and is beneficial in case of hardware limitations, such as limited computational resources.

For future work, we will investigate the extension of the approach for more sophisticated constraints between agents. We will also study the extension to multi-agents while systematically developing robust optimal control algorithms to address switching in hybrid models. As an alternative research direction, we will explore how to take benefit from cooperation and interaction forces for traversing highly tilted floors that cannot be achieved with single-agent robots.

REFERENCES

[1] J. Kim and K. Akbari Hamed, "Cooperative locomotion via supervisory predictive control and distributed nonlinear controllers," *Journal of Dynamic Systems, Measurement, and Control*, vol. 144, no. 3, p. 031005, Mar. 2022.

[2] A. Agrawal, O. Harib, A. Hereid, S. Finet, M. Masselin, L. Praly, A. Ames, K. Sreenath, and J. Grizzle, "First steps towards translating HZD control of bipedal robots to decentralized control of exoskeletons," *IEEE Access*, vol. 5, pp. 9919–9934, 2017.

[3] K. Akbari Hamed and R. D. Gregg, "Decentralized event-based controllers for robust stabilization of hybrid periodic orbits: Application to underactuated 3D bipedal walking," *IEEE Transactions on Automatic Control*, vol. 64, no. 6, pp. 2266–2281, June 2019.

[4] R. Gregg and J. Sensinger, "Towards biomimetic virtual constraint control of a powered prosthetic leg," *IEEE Transactions on Control Systems Technology*, vol. 22, no. 1, pp. 246–254, Jan 2014.

[5] H. Zhao, J. Horn, J. Reher, V. Paredes, and A. D. Ames, "Multicontact locomotion on transfemoral prostheses via hybrid system models and optimization-based control," *IEEE Transactions on Automation Science and Engineering*, vol. 13, no. 2, pp. 502–513, 2016.

[6] K. Akbari Hamed, V. R. Kamidi, W. Ma, A. Leonessa, and A. D. Ames, "Hierarchical and safe motion control for cooperative locomotion of robotic guide dogs and humans: A hybrid systems approach," *IEEE Robotics and Automation Letters*, vol. 5, no. 1, pp. 56–63, Jan 2020.

[7] E. Tuci, M. H. Alkilabi, and O. Akanyeti, "Cooperative object transport in multi-robot systems: A review of the state-of-the-art," *Frontiers in Robotics and AI*, vol. 5, p. 59, 2018.

[8] Z. Yan, N. Jouandeau, and A. A. Cherif, "A survey and analysis of multi-robot coordination," *International Journal of Advanced Robotic Systems*, vol. 10, no. 12, p. 399, 2013.

[9] K. Bouyarmane, K. Chappellet, J. Vaillant, and A. Kheddar, "Quadratic programming for multirobot and task-space force control," *IEEE Transactions on Robotics*, vol. 35, no. 1, pp. 64–77, 2018.

[10] R. M. Murray, Z. Li, and S. S. Sastry, *A mathematical introduction to robotic manipulation*. CRC press, 2017.

[11] D. Williams and O. Khatib, "The virtual linkage: A model for internal forces in multi-grasp manipulation," in *Proceedings IEEE International Conference on Robotics and Automation*, 1993, pp. 1025–1030.

[12] P. Culbertson, J.-J. Slotine, and M. Schwager, "Decentralized adaptive control for collaborative manipulation of rigid bodies," *IEEE Transactions on Robotics*, vol. 37, no. 6, pp. 1906–1920, 2021.

[13] S. Erhart, D. Sieber, and S. Hirche, "An impedance-based control architecture for multi-robot cooperative dual-arm mobile manipulation," in *IEEE/RSJ International Conference on Intelligent Robots and Systems*, 2013, pp. 315–322.

[14] J. Alonso-Mora, S. Baker, and D. Rus, "Multi-robot formation control and object transport in dynamic environments via constrained optimization," *The International Journal of Robotics Research*, vol. 36, no. 9, pp. 1000–1021, 2017.

[15] M. L. Elwin, B. Strong, R. A. Freeman, and K. M. Lynch, "Human-multirobot collaborative mobile manipulation: the omnid mocobots," *IEEE Robotics and Automation Letters*, vol. 8, no. 1, pp. 376–383, 2022.

[16] Y. Chen, A. Singletary, and A. D. Ames, "Guaranteed obstacle avoidance for multi-robot operations with limited actuation: A control barrier function approach," *IEEE Control Systems Letters*, vol. 5, no. 1, pp. 127–132, 2020.

[17] K. Sreenath and V. Kumar, "Dynamics, control and planning for cooperative manipulation of payloads suspended by cables from multiple quadrotor robots," in *Proceedings of Robotics: Science and Systems*, Berlin, Germany, June 2013.

[18] C. Masone, H. H. Bülthoff, and P. Stegagno, "Cooperative transportation of a payload using quadrotors: A reconfigurable cable-driven parallel robot," in *IEEE/RSJ International Conference on Intelligent Robots and Systems*, 2016, pp. 1623–1630.

[19] P. O. Pereira and D. V. Dimarogonas, "Collaborative transportation of a bar by two aerial vehicles with attitude inner loop and experimental validation," in *IEEE Conference on Decision and Control*, 2017, pp. 1815–1820.

[20] G. Li, R. Ge, and G. Loianno, "Cooperative transportation of cable suspended payloads with MAVs using monocular vision and inertial sensing," *IEEE Robotics and Automation Letters*, vol. 6, no. 3, pp. 5316–5323, 2021.

[21] D. Mellinger, M. Shomin, N. Michael, and V. Kumar, "Cooperative grasping and transport using multiple quadrotors," in *Distributed Autonomous Robotic Systems*. Springer, 2013, pp. 545–558.

[22] H.-N. Nguyen, S. Park, J. Park, and D. Lee, "A novel robotic platform for aerial manipulation using quadrotors as rotating thrust generators," *IEEE Transactions on Robotics*, vol. 34, no. 2, pp. 353–369, 2018.

[23] A. Tagliabue, M. Kamel, R. Siegwart, and J. Nieto, "Robust collaborative object transportation using multiple MAVs," *The International Journal of Robotics Research*, vol. 38, no. 9, pp. 1020–1044, 2019.

[24] J. Wehbeh, S. Rahman, and I. Sharf, "Distributed model predictive control for UAVs collaborative payload transport," in *IEEE/RSJ International Conference on Intelligent Robots and Systems*, 2020, pp. 11 666–11 672.

[25] F. Caccavale, G. Giglio, G. Muscio, and F. Pierri, "Cooperative impedance control for multiple UAVs with a robotic arm," in *IEEE/RSJ International Conference on Intelligent Robots and Systems*, 2015, pp. 2366–2371.

[26] H. Yang and D. Lee, "Hierarchical cooperative control framework of multiple quadrotor-manipulator systems," in *IEEE International Conference on Robotics and Automation*, 2015, pp. 4656–4662.

[27] H. Lee, H. Kim, W. Kim, and H. J. Kim, "An integrated framework for cooperative aerial manipulators in unknown environments," *IEEE Robotics and Automation Letters*, vol. 3, no. 3, pp. 2307–2314, 2018.

[28] D. Panagou, M. Turpin, and V. Kumar, "Decentralized goal assignment and safe trajectory generation in multirobot networks via multiple Lyapunov functions," *IEEE Transactions on Automatic Control*, vol. 65, no. 8, pp. 3365–3380, 2020.

[29] J. Spletzer, A. K. Das, R. Fierro, C. J. Taylor, V. Kumar, and J. P. Ostrowski, "Cooperative localization and control for multi-robot manipulation," in *Proceedings IEEE/RSJ International Conference on Intelligent Robots and Systems. Expanding the Societal Role of Robotics in the the Next Millennium (Cat. No. 01CH37180)*, vol. 2, 2001, pp. 631–636.

[30] G. A. Pereira, M. F. Campos, and V. Kumar, "Decentralized algorithms for multi-robot manipulation via caging," *The International Journal of Robotics Research*, vol. 23, no. 7-8, pp. 783–795, 2004.

[31] H. Farivarnejad, S. Wilson, and S. Berman, "Decentralized sliding mode control for autonomous collective transport by multi-robot systems," in *IEEE Conference on Decision and Control*, 2016, pp. 1826–1833.

[32] T. Machado, T. Malheiro, S. Monteiro, W. Erlhagen, and E. Bicho, "Multi-constrained joint transportation tasks by teams of autonomous mobile robots using a dynamical systems approach," in *IEEE International Conference on Robotics and Automation*, 2016, pp. 3111–3117.

[33] M. Mesbahi and M. Egerstedt, *Graph Theoretic Methods in Multiagent Networks*. Princeton University Press, 2010.

[34] F. Bullo, J. Cortés, and S. Martinez, *Distributed Control of Robotic Networks: A Mathematical Approach to Motion Coordination Algorithms*. Princeton University Press, 2009.

[35] W. B. Dunbar and R. M. Murray, "Distributed receding horizon control for multi-vehicle formation stabilization," *Automatica*, vol. 42, no. 4, pp. 549–558, 2006.

[36] J. M. Maestre and R. R. Negenborn, *Distributed Model Predictive Control Made Easy*. Springer, 2014.

[37] M. Ahmadi, A. Singletary, J. W. Burdick, and A. D. Ames, "Safe policy synthesis in multi-agent POMDPs via discrete-time barrier functions," in *IEEE Conference on Decision and Control*, 2019, pp. 4797–4803.

[38] M. Tranzatto, T. Miki, M. Dharmadhikari, L. Bernreiter, M. Kulkarni, F. Mascarich, O. Andersson, S. Khattak, M. Hutter, R. Siegwart, and K. Alexis, "CERBERUS in the DARPA subterranean challenge," *Science Robotics*, vol. 7, no. 66, p. eabp9742, 2022.

[39] C. Yang, G. N. Sue, Z. Li, L. Yang, H. Shen, Y. Chi, A. Rai, J. Zeng, and K. Sreenath, "Collaborative navigation and manipulation of a cable-towed load by multiple quadrupedal robots," *IEEE Robotics and Automation Letters*, vol. 7, no. 4, pp. 10 041–10 048, 2022.

[40] K. Akbari Hamed, V. R. Kamidi, A. Pandala, W. Ma, and A. D. Ames, "Distributed feedback controllers for stable cooperative locomotion of quadrupedal robots: A virtual constraint approach," in *American Control Conference*, 2020, pp. 5314–5321.

[41] R. Full and D. Koditschek, "Templates and anchors: Neuromechanical hypotheses of legged locomotion on land," *Journal of Experimental Biology*, vol. 202, no. 23, pp. 3325–3332, 1999.

[42] S. Kajita and K. Tani, "Study of dynamic biped locomotion on rugged terrain-derivation and application of the linear inverted pendulum mode," in *IEEE International Conference on Robotics and Automation*, 1991, pp. 1405–1406.

[43] D. E. Orin, A. Goswami, and S.-H. Lee, "Centroidal dynamics of a humanoid robot," *Autonomous robots*, vol. 35, no. 2, pp. 161–176, 2013.

[44] G. Bledt, M. J. Powell, B. Katz, J. Di Carlo, P. M. Wensing, and S. Kim, "MIT Cheetah 3: Design and control of a robust, dynamic quadruped robot," in *IEEE/RSJ International Conference on Intelligent Robots and Systems*, Oct 2018, pp. 2245–2252.

[45] M. Chignoli and P. M. Wensing, "Variational-based optimal control of underactuated balancing for dynamic quadrupeds," *IEEE Access*, vol. 8, pp. 49 785–49 797, 2020.

[46] Y. Ding, A. Pandala, C. Li, Y.-H. Shin, and H.-W. Park, "Representation-free model predictive control for dynamic motions in quadrupeds," *IEEE Transactions on Robotics*, vol. 37, no. 4, pp. 1154–1171, 2021.

[47] R. J. Griffin, G. Wiedebach, S. Bertrand, A. Leonessa, and J. Pratt, "Walking stabilization using step timing and location adjustment on the humanoid robot, Atlas," in *IEEE/RSJ International Conference on Intelligent Robots and Systems*, Sep. 2017, pp. 667–673.

[48] J. Englsberger, C. Ott, M. A. Roa, A. Albu-Schäffer, and G. Hirzinger, "Bipedal walking control based on capture point dynamics," in *IEEE/RSJ International Conference on Intelligent Robots and Systems (IROS)*, Sep. 2011, pp. 4420–4427.

[49] J. Pratt, J. Carff, S. Drakunov, and A. Goswami, "Capture point: A step toward humanoid push recovery," in *IEEE-RAS International Conference on Humanoid Robots*, 2006, pp. 200–207.

[50] H. Dai, A. Valenzuela, and R. Tedrake, "Whole-body motion planning with centroidal dynamics and full kinematics," in *IEEE-RAS International Conference on Humanoid Robots*, 2014, pp. 295–302.

[51] J. Di Carlo, P. M. Wensing, B. Katz, G. Bledt, and S. Kim, "Dynamic locomotion in the MIT Cheetah 3 through convex model-predictive control," in *IEEE/RSJ International Conference on Intelligent Robots and Systems*, Oct 2018, pp. 1–9.

[52] R. Grandia, F. Farshidian, A. Dosovitskiy, R. Ranftl, and M. Hutter, "Frequency-aware model predictive control," *IEEE Robotics and Automation Letters*, vol. 4, no. 2, pp. 1517–1524, 2019.

[53] K. Akbari Hamed, J. Kim, and A. Pandala, "Quadrupedal locomotion via event-based predictive control and QP-based virtual constraints," *IEEE Robotics and Automation Letters*, vol. 5, no. 3, pp. 4463–4470, 2020.

[54] R. T. Fawcett, A. Pandala, J. Kim, and K. Akbari Hamed, "Real-time planning and nonlinear control for quadrupedal locomotion with articulated tails," *Journal of Dynamic Systems, Measurement, and Control*, vol. 143, no. 7, p. 071004, July 2021.

[55] F. Farshidian, M. Neunert, A. W. Winkler, G. Rey, and J. Buchli, "An efficient optimal planning and control framework for quadrupedal locomotion," in *IEEE International Conference on Robotics and Automation*, 2017, pp. 93–100.

[56] A. Pandala, R. T. Fawcett, U. Rosolia, A. D. Ames, and K. Akbari Hamed, "Robust predictive control for quadrupedal locomotion: Learning to close the gap between reduced-and full-order models," *IEEE Robotics and Automation Letters*, vol. 7, no. 3, pp. 6622–6629, 2022.

[57] J. Grizzle, G. Abba, and F. Plestan, "Asymptotically stable walking for biped robots: Analysis via systems with impulse effects," *IEEE Transactions on Automatic Control*, vol. 46, no. 1, pp. 51–64, Jan 2001.

[58] E. R. Westervelt, J. W. Grizzle, C. Chevallereau, J. H. Choi, and B. Morris, *Feedback control of dynamic bipedal robot locomotion*. CRC press, 2018.

[59] Y. Hurmuzlu and D. B. Marghitu, "Rigid body collisions of planar kinematic chains with multiple contact points," *The International Journal of Robotics Research*, vol. 13, no. 1, pp. 82–92, 1994.

[60] B. Morris and J. Grizzle, "Hybrid invariant manifolds in systems with impulse effects with application to periodic locomotion in bipedal robots," *IEEE Transactions on Automatic Control*, vol. 54, no. 8, pp. 1751–1764, Aug 2009.

[61] I. Poulakakis and J. Grizzle, "The spring loaded inverted pendulum as the hybrid zero dynamics of an asymmetric hopper," *IEEE Transactions on Automatic Control*, vol. 54, no. 8, pp. 1779–1793, Aug 2009.

[62] W. Haddad, V. Chellaboina, and S. Nersesov, *Impulsive and Hybrid Dynamical Systems: Stability, Dissipativity, and Control*. Princeton University Press, July 2006.

[63] R. Goebel, R. Sanfelice, and A. Teel, *Hybrid Dynamical Systems: Modeling, Stability, and Robustness*. Princeton University Press, March 2012.

[64] A. M. Johnson, S. A. Burden, and D. E. Koditschek, "A hybrid systems model for simple manipulation and self-manipulation systems," *The International Journal of Robotics Research*, vol. 35, no. 11, pp. 1354–1392, 2016.

[65] M. Spong, J. Holm, and D. Lee, "Passivity-based control of bipedal locomotion," *IEEE Robotics Automation Magazine*, vol. 14, no. 2, pp. 30–40, June 2007.

[66] A. D. Ames, R. D. Gregg, E. D. Wendel, and S. Sastry, "On the geometric reduction of controlled three-dimensional bipedal robotic walkers," in *Lagrangian and Hamiltonian Methods for Nonlinear Control 2006*. Springer, 2007, pp. 183–196.

[67] M. Spong and F. Bullo, "Controlled symmetries and passive walking," *IEEE Transactions on Automatic Control*, vol. 50, no. 7, pp. 1025–1031, July 2005.

[68] I. Manchester, U. Mettin, F. Iida, and R. Tedrake, "Stable dynamic walking over uneven terrain," *The International Journal of Robotics Research*, vol. 30, no. 3, pp. 265–279, 2011.

[69] A. Ames, K. Galloway, K. Sreenath, and J. Grizzle, "Rapidly exponentially stabilizing control Lyapunov functions and hybrid zero dynamics," *IEEE Transactions on Automatic Control*, vol. 59, no. 4, pp. 876–891, April 2014.

[70] E. Westervelt, J. Grizzle, and D. Koditschek, "Hybrid zero dynamics of planar biped walkers," *IEEE Transactions on Automatic Control*, vol. 48, no. 1, pp. 42–56, Jan 2003.
[71] A. Isidori, *Nonlinear Control Systems*. Springer; 3rd edition, 1995.
[72] C. Chevallereau, G. Abba, Y. Aoustin, F. Plestan, E. Westervelt, C. Canudas-de Wit, and J. Grizzle, "RABBIT: A testbed for advanced control theory," *IEEE Control Systems Magazine*, vol. 23, no. 5, pp. 57–79, Oct 2003.
[73] K. Sreenath, H.-W. Park, I. Poulakakis, and J. Grizzle, "Embedding active force control within the compliant hybrid zero dynamics to achieve stable, fast running on MABEL," *The International Journal of Robotics Research*, vol. 32, no. 3, pp. 324–345, 2013.
[74] X. Da and J. Grizzle, "Combining trajectory optimization, supervised machine learning, and model structure for mitigating the curse of dimensionality in the control of bipedal robots," *The International Journal of Robotics Research*, vol. 38, no. 9, pp. 1063–1097, 2019.
[75] A. Hereid, C. M. Hubicki, E. A. Cousineau, and A. D. Ames, "Dynamic humanoid locomotion: A scalable formulation for HZD gait optimization," *IEEE Transactions on Robotics*, vol. 34, no. 2, pp. 370–387, 2018.
[76] A. E. Martin, D. C. Post, and J. P. Schmiedeler, "The effects of foot geometric properties on the gait of planar bipeds walking under HZD-based control," *The International Journal of Robotics Research*, vol. 33, no. 12, pp. 1530–1543, 2014.
[77] R. T. Fawcett, A. Pandala, A. D. Ames, and K. Akbari Hamed, "Robust stabilization of periodic gaits for quadrupedal locomotion via QP-based virtual constraint controllers," *IEEE Control Systems Letters*, pp. 1736–1741, 2021.
[78] W.-L. Ma, N. Csomay-Shanklin, S. Kolathaya, K. Akbari Hamed, and A. D. Ames, "Coupled control Lyapunov functions for interconnected systems, with application to quadrupedal locomotion," *IEEE Robotics and Automation Letters*, vol. 6, no. 2, pp. 3761–3768, 2021.
[79] M. Posa, S. Kuindersma, and R. Tedrake, "Optimization and stabilization of trajectories for constrained dynamical systems," in *IEEE International Conference on Robotics and Automation*, May 2016, pp. 1366–1373.
[80] J. Carpentier, S. Tonneau, M. Naveau, O. Stasse, and N. Mansard, "A versatile and efficient pattern generator for generalized legged locomotion," in *IEEE International Conference on Robotics and Automation*, May 2016, pp. 3555–3561.
[81] M. Kelly, "An introduction to trajectory optimization: How to do your own direct collocation," *SIAM Review*, vol. 59, no. 4, pp. 849–904, 2017.
[82] A. Patel, S. L. Shield, S. Kazi, A. M. Johnson, and L. T. Biegler, "Contact-implicit trajectory optimization using orthogonal collocation," *IEEE Robotics and Automation Letters*, vol. 4, no. 2, pp. 2242–2249, 2019.
[83] R. T. Fawcett, K. Afsari, A. D. Ames, and K. Akbari Hamed, "Toward a data-driven template model for quadrupedal locomotion," *IEEE Robotics and Automation Letters*, vol. 7, no. 3, pp. 7636–7643, 2022.
[84] C. D. Bellicoso, C. Gehring, J. Hwangbo, P. Fankhauser, and M. Hutter, "Perception-less terrain adaptation through whole body control and hierarchical optimization," in *IEEE-RAS International Conference on Humanoid Robots*, 2016, pp. 558–564.
[85] L. Hawley and W. Suleiman, "Control framework for cooperative object transportation by two humanoid robots," *Robotics and Autonomous Systems*, vol. 115, pp. 1–16, 2019.
[86] M.-H. Wu, A. Konno, S. Ogawa, and S. Komizunai, "Symmetry cooperative object transportation by multiple humanoid robots," in *IEEE International Conference on Robotics and Automation (ICRA)*, 2014, pp. 3446–3451.
[87] M. Vukobratović, B. Borovac, and D. Surla, *Dynamics of Biped Locomotion*. Springer, 1990.
[88] F. Borrelli, A. Bemporad, and M. Morari, *Predictive Control for Linear and Hybrid Systems*. Cambridge University Press, 2017.
[89] Y. Wang and S. Boyd, "Fast model predictive control using online optimization," *IEEE Transactions on Control Systems Technology*, vol. 18, no. 2, pp. 267–278, March 2010.
[90] M. H. Raibert, *Legged robots that balance*. MIT press, 1986.
[91] V. R. Kamidi, J. Kim, R. T. Fawcett, A. D. Ames, and K. Akbari Hamed, "Distributed quadratic programming-based nonlinear controllers for periodic gaits on legged robots," *IEEE Control Systems Letters*, vol. 6, pp. 2509–2514, 2022.
[92] J. Hwangbo, J. Lee, and M. Hutter, "Per-contact iteration method for solving contact dynamics," *IEEE Robotics and Automation Letters*, vol. 3, no. 2, pp. 895–902, April 2018.
[93] A. G. Pandala, Y. Ding, and H. Park, "qpSWIFT: A real-time sparse quadratic program solver for robotic applications," *IEEE Robotics and Automation Letters*, vol. 4, no. 4, pp. 3355–3362, Oct 2019.
[94] Layered control for cooperative locomotion of two quadrupedal robots. [Online]. Available: https://youtu.be/ZNcrOmzKu44.

Jeeseop Kim (Member, IEEE) received his B.S. in mechanical and aerospace engineering and his M.S. in intelligence and information from Seoul National University in 2014 and 2017, respectively. He obtained his Ph.D. in mechanical engineering from Virginia Tech, Blacksburg, VA, USA, in 2022. He is currently working as a Postdoctoral Research Associate in Mechanical and Civil Engineering at Caltech, Pasadena, CA, USA. His research interests include nonlinear control, safety-critical control, and optimization-based control with applications to collaborative legged robots.

Randall T. Fawcett obtained his B.S. in mechanical engineering from Auburn University in 2019, focusing on control and biomechanics. He received his M.S. in mechanical engineering at Virginia Tech in 2021. He received his Ph.D. at Virginia Tech in 2023, where his research focused on the intersection of data-driven control, optimal control, and trajectory planning for multi-agent legged robotic systems. He is currently an Engineering Consultant at Exponent.

Vinay R. Kamidi received his M.S. and Ph.D. in mechanical engineering from Virginia Tech, Blacksburg, VA, USA, in 2018 and 2022, respectively. He is currently working as a Senior Software and Controls Engineer at Apptronik in Austin, Texas. His research interest focuses on nonlinear control, decentralized/distributed control, safety-critical control, optimization, and experimental realization on quadrupedal and bipedal robots.

Aaron D. Ames (Fellow, IEEE) is the Bren Professor of Mechanical and Civil Engineering and Control and Dynamical Systems at Caltech. He received a B.S. in Mechanical Engineering and a B.A. in Mathematics from the University of St. Thomas in 2001, and he received an M.A. in Mathematics and a Ph.D. in Electrical Engineering and Computer Sciences from UC Berkeley in 2006. He served as a Postdoctoral Scholar in Control and Dynamical Systems at Caltech from 2006 to 2008 and began his faculty career at Texas A&M University in 2008. Prior to joining Caltech, he was an Associate Professor in Mechanical Engineering and Electrical & Computer Engineering at the Georgia Institute of Technology. At UC Berkeley, he was the recipient of the 2005 Leon O. Chua Award for achievement in nonlinear science and the 2006 Bernard Friedman Memorial Prize in Applied Mathematics, and he received the NSF CAREER award in 2010, the 2015 Donald P. Eckman Award, and the 2019 Antonio Ruberti Young Researcher Prize. His research interests span the areas of robotics, nonlinear, safety-critical control, and hybrid systems, with a special focus on applications to bipedal robotic walking—both formally and through experimental validation. His lab designs, builds, and tests novel bipedal robots, humanoids, prostheses, and exoskeletons with the goal of achieving dynamic locomotion on legged robots and translating these capabilities into robotic assistive devices. The application of these ideas ranges from increased autonomy in robots to improving the locomotion capabilities of the mobility impaired.

Kaveh Akbari Hamed (Member, IEEE) received the B.S. degree in electrical engineering from the University of Tabriz, Tabriz, Iran, in 2004, and the M.S. and Ph.D. degrees in electrical engineering from the Sharif University of Technology, Tehran, Iran, in 2006 and 2011, respectively. He was a Postdoctoral Research Fellow working with the Department of Electrical Engineering and Computer Science, University of Michigan, from 2012 to 2014. He is currently an Associate Professor in mechanical engineering at Virginia Tech, Blacksburg, VA, USA. His research interests include nonlinear and robust control, distributed/decentralized control, model predictive control, legged robots, and hybrid systems.